THE INFLUENCE OF DEPTH OF SUBMERSION, ASPECT RATIO, AND THICKNESS ON SUPERCAVITATING HYDROFOILS OPERATING AT ZERO CAVITATION NUMBER

Virgil E. Johnson, Jr.
Langley Research Center
National Aeronautic and Space Administration

* * * * *

The linearized theory for infinite depth is applied to design two new low-drag supercavitating hydrofoils. The linearized solution for the characteristics of supercavitating hydrofoils operating at zero cavitation number at finite depth is also accomplished. The effects of camber determined from the linear theory are combined with the exact nonlinear flat-plate solution to produce nonlinear expressions for the characteristics of arbitrary sections. The resulting theoretical expressions are corrected for aspect ratio by conventional aeronautical methods. Agreement between theory and experiment is found to be good for the lift coefficient, drag coefficient, center of pressure, and location of the upper cavity streamline. The theory is used to compare the maximum lift/drag ratios obtainable from various cambered sections of equal strength. At an aspect ratio of 3 and a depth of 1 chord, a five-term section with $C_{L,d} = 0.1$ has a maximum L/D of 10.5. However, the maximum L/D is not greatly dependent on the type of camber since a circular arc section of $C_{L,d} = 0.1$ has a maximum L/D of about 9.5. It is concluded from the analysis that for operation at a depth greater than about 1 chord, a lift/drag ratio of about 10 is close to the maximum value that can ever be attained on a single hydrofoil supported with one strut and operating at zero cavitation number.

* * * * *

INTRODUCTION

One of the missions of the Hydrodynamics Division of the National Aeronautics and Space Administration is to find means of improving the takeoff and landing performance of seaplanes, particularly in rough water. The desirability of using an auxiliary lifting surface such as a hydro-ski for reducing seaplane hull loads and improving rough water performance has been established. It is possible that hydrofoils with higher aspect ratio and thus higher efficiencies could be superior to the hydro-ski; however, only the low-aspect-ratio planing hydro-ski has so far been successfully applied as landing gear to modern high-speed aircraft. This is because the conventional hydrofoil presents problems not experienced by a hydro-ski.

As a hydrofoil nears the free surface (during a takeoff run) the low pressure side of the foil almost always becomes ventilated from the atmosphere. This phenomenon results in a severe and usually abrupt loss in lift and reduction in the lift/drag ratio. For conventional airfoil sections the loss in lift may exceed 75 percent. The speed at the inception of ventilation depends on the angle of attack and depth of submersion; but, except for very small angles of attack and relatively low takeoff speeds, the inception speed is usually well below the takeoff speed of the aircraft.

Even if the ventilation problem is overcome by using small angles of attack and incorporating "fences" or other devices for suppressing ventilation, the onset of cavitation presents a second deterrent to the use of conventional hydrofoils at high speeds. The loss in lift accompanying cavitation of conventional airfoil sections is not abrupt, but the ultimate reduction in lift and lift/drag ratio is comparable to that of ventilated flow. Even thin airfoil sections of small design lift coefficient enter this cavitating regime of poor lift/drag ratios at speeds in excess of about 80 knots.

Since the takeoff speed of supersonic aircraft may be in the range of 150 to 200 knots, lifting surfaces with cavitating or ventilating characteristics superior to those of conventional airfoil sections are desirable. Fortunately the theoretical work of Tulin and Burkart (1) has shown that superior configurations do exist, and they have selected a cambered configuration for operation in cavitating or ventilated flow which has two-dimensional lift/drag ratios at its design angle of attack and zero cavitation number about six times that of a flat plate. If such a cambered foil can be induced to ventilate at very low speeds, while the aircraft hull still supports most of the load, a stable and efficient takeoff run may be possible. This new philosophy is to design for operation with a cavity; whereas in the past the philosophy has been to try to avoid cavitation and ventilation. The situation is very definitely one of, "If you can't beat it, join it."

The present paper is concerned with some theoretical and experimental work on supercavitating hydrofoils which has been carried out during the last few years at the Langley Research Center, Langley Field, Virginia, of the National Aeronautics and Space Administration. A large percentage of the information contained in this paper has been previously published as Refs. 2 and 3. However, since these reports have only recently been declassified, the principal results contained in them are reviewed, although in some places details are omitted. The purpose of the investigation has been to determine the characteristics of practical supercavitating hydrofoils; therefore the effects of aspect ratio, depth of submersion, and hydrofoil thickness are subjects of particular interest. The theoretical portion makes frequent use of the linearized theory for cavitating flows developed in Ref. 1 and extends this theory to include the problem of hydrofoils which operate in a ventilated condition near the free surface. Conventional aeronautical corrections for finite span are employed. The theoretical results obtained are compared with a variety of experimental data obtained in the towing tanks of the NASA. These tanks include the new high-speed facility which is presently capable of speeds up to 175 fps and which will soon be capable of speeds nearing 260 fps.

SYMBOLS

A aspect ratio

A_n, A_0 coefficients of sine-series expansion of vorticity distribution on equivalent airfoil section, that is,

$$\Omega(x) = 2V \left(A_0 \cot \frac{\theta}{2} + A_1 \sin \theta + A_2 \sin 2\theta \cdots A_n \sin n\theta\right)$$

where

$$A_n = \frac{2}{\pi}\int_0^{\pi} \frac{d\bar{y}}{d\bar{x}} \cos n\theta \, d\theta$$

$$A_0 = -\frac{1}{\pi}\int_0^{\pi} \frac{d\bar{y}}{d\bar{x}} \, d\theta + \alpha = \alpha + A_0'$$

$A_{n,h}, A_{0,h}$ coefficients of sine-series expansion of vorticity distribution on hydrofoil section

a distance from equivalent airfoil leading edge to center of pressure in chords

B_n, B_0 coefficients of cosine series defining location of image vortex in airfoil plane using $z = -\sqrt{Z}$ transformation

b parameter defining location of spray at infinity in t plane (see Ref. 4)

C_D total drag coefficient, D/qS

C_f skin-friction drag coefficient, D_f/qS

C_L total-lift coefficient, L/qS

$\bar{C}_L$ total-lift coefficient of equivalent airfoil section, $\bar{L}/\bar{q}\bar{S}$

$C_{L,1}$ lift coefficient exclusive of crossflow, L_1/qS

$C_{L,c}$ crossflow lift coefficient, L_c/qS

C_m pitching-moment coefficient (about the leading edge), M/qSc

$\bar{C}_m$ pitching-moment coefficient of equivalent airfoil section (about the leading edge), $\bar{M}/qSc$

$\bar{C}_{m,3}$ third-moment coefficient of equivalent airfoil section (see Ref. 1), $\bar{M}_3/qSc^4$

C_N resultant-force coefficient on arbitrary section, F/qS

$C_{N,f}$ resultant-force coefficient of flat plate, F/qS

C_n, C_0 coefficients of sine-series expansion of vorticity distribution on equivalent airfoil section at arbitrary depth using $Z = -\sqrt{Z}$ transformation

C_p pressure coefficient, $(p - p_\infty)/q$

c chord

D total drag force

D_f drag force due to skin friction

d leading edge depth of submersion

E Jones' edge correction, ratio of semiperimeter to span (see Ref. 5)

F resultant force

f distance from hydrofoil leading edge to stagnation point in chords

g acceleration due to gravity

L total lift force

L_c lift force due to crossflow

L_1 lift force exclusive of crossflow, $L - L_c$

ℓ perpendicular distance from hydrofoil reference line to upper cavity streamline

M moment about leading edge

$\overline{M}_3$ third moment about leading edge, $2 \int_0^{\overline{c}} p(\overline{x})\, \overline{x}^3\, d\overline{x}$

$m = C_L/\alpha$

p pressure, lb/sq ft

p_c pressure within cavity, lb/sq ft

p_o pressure at mean depth of hydrofoil, lb/sq ft

p_v fluid vapor pressure, lb/sq ft

q free-stream dynamic pressure, $1/2\, \rho V^2$

R cavity ordinate - aspect ratio correction factor

S area, sq ft

s span, ft

u perturbation velocity in X-direction

V speed of advance, fps

v perturbation velocity in Y-direction

X, Y coordinate axes

x distance from leading edge along X-axis

$x_{c.p.}$ distance from leading edge to center of pressure of hydrofoil

α geometric angle of attack measured from reference line radians unless otherwise specified

α_c angle-of-attack increase due to camber, radians unless otherwise specified

α_i induced angle of attack, radians unless otherwise specified

α_o angle between hydrofoil chord line and reference line, positive when chord line is below the reference line, radians unless otherwise specified

α' angle of attack measured from hydrofoil chord line, $\alpha' = \alpha + \alpha_o$, radians unless otherwise specified

Γ circulation, strength of single vortex

γ central angle subtending chord of circular-arc hydrofoil

δ spray thickness at infinite distance downstream

ϵ deviation of resultant force vector from normal to hydrofoil reference line

ζ complex airfoil plane, η-ξ plane

η ordinate in the ζ plane

θ parameter defining distance along airfoil chord, $\bar{x} = \bar{c}/2\ (1 - \cos\theta)$

ρ mass density, $\mathrm{lb\text{-}sec^2/ft^4}$

ξ abscissa in the ζ plane

σ cavitation number, $(p_o - p_c)/q$

σ_i cavitation number at inception

τ correction factor for variation from elliptical plan form

φ angle between spray and horizontal

Ω vorticity

{ } indicates "function of," for example, $C_N\{\alpha\} = C_{N,f}\{\alpha + \alpha_c\}$ also () sometimes used

$Z = X + iY$

$\beta = \tan^{-1}\dfrac{C_D}{C_L} = \alpha + \epsilon$

Subscripts

e effective

0 zero depth of submersion

t total

∞ infinite depth of submersion

c.p. center of pressure

c due to camber

A_o due to A_o

Barred symbols refer to equivalent airfoil section and unbarred symbols refer to the supercavitating hydrofoil section.

DESCRIPTION OF SUPERCAVITATING FLOW

The parameter defining cavity flow is $\sigma = (p_o - p_c)/q$ where p_o is the pressure at the mean depth, p_c is the pressure within the cavity, and q is the dynamic pressure. The magnitude of σ for the condition at which cavitation is incipient is defined by the particular value σ_i. If σ is reduced below σ_i, cavitation becomes more severe; that is, the cavitation zone extends over a larger area. When a hydrofoil operates at sufficiently low values of σ, the cavity formed may completely enclose the upper or suction surface and extend several chords downstream as shown in Fig. 1a. The re-entrant flow formed at the rear of the cavity is caused by the necessity for constant pressure along the cavity streamline. When the cavity is sufficiently long so that the re-entrant flow is dissipated without impinging on the body creating the cavity as shown in Fig. 1a, the flow is defined as supercavitating. Theoretically, if the cavitation parameter is reduced to zero the cavity formed will extend to infinity.

Low values of cavitation number, and thus supercavitating flow, may be obtained by increasing either velocity or cavity pressure or both. At a constant depth and water temperature, σ for normal vapor-filled cavities is dependent only on the velocity, since $p_o - p_c$ is then $p_o - p_v$ and is constant.

If part or all of the boundary layer of a configuration is separated, the eddying fluid in the separated region can be replaced by a continuous flow of lighter fluid such as air (6,7). Regulation of the amount of air supplied will control the cavity pressure and thus the length of the cavity formed. If the quantity of air supplied is very large, the cavity pressure will approach the ambient pressure p_o and a very long cavity will result even at low stream velocities.

The ventilation of surface-piercing hydrofoils is therefore a supercavitating flow due to large quantities of air supplied from the atmosphere to separated flow on the suction surface of the foil. Supercavitating flow as a result of ventilation also occurs when a non-surface-piercing hydrofoil of moderate aspect-ratio operates near the free surface (Fig. 1b). As pointed out in Ref. 8, air is entrained in the trailing vortices and drawn to the suction side of the foil, causing a long trailing cavity to completely enclose the foil upper surface and extend far downstream. The ventilated-type cavity described in Ref. 8 differs in shape from those formed in deeply submerged flow because of the proximity of the free surface. It is similar to planing, with the spray forming the upper surface of the cavity. Since the cavity pressure is

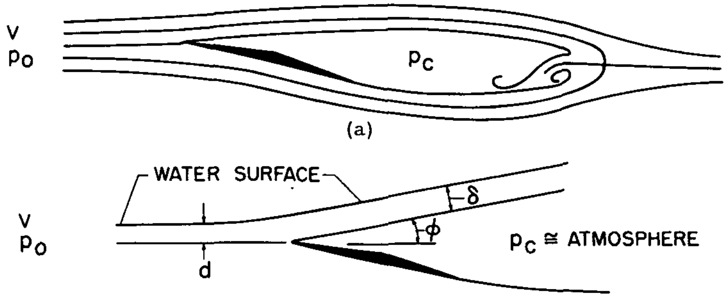

Fig. 1 - Definition sketch: (a) supercavitating flow at finite cavitation number ($\sigma > 0$), (b) supercavitating or ventilated flow near the free surface ($\sigma \simeq 0$)

approximately the same as the ambient pressure (at small depths of submersion), the cavitation number for this type flow is nearly zero. The present paper is concerned with the theoretical predictions of the characteristics of practical hydrofoils operating in the ventilated or zero-cavitation-number regime.

FORCES AND MOMENTS

Two-Dimensional Theory

Flat Plate, Infinite Depth—The characteristics of a two-dimensional inclined flat plate in an infinite fluid, operating at zero cavitation number, have been obtained by Kirchoff and Rayleigh (9). The resultant force on the platé is given by the well-known equation

$$C_{n,f} = \frac{2\pi \sin \alpha}{4 + \pi \sin \alpha}. \tag{1}$$

Flat Plate, Finite Depth—Similar work was performed by A. E. Green (4,10) to include the effect of the free surface (but neglecting gravity). The solution is necessarily obtained in terms of spray thickness δ rather than the more useful depth of submersion and is given as two parametric equations in terms of the parameter b:

$$C_L = C_{N,f} \cos \alpha = \frac{2\left(b - \sqrt{b^2 - 1}\right) \sin \alpha \cos \alpha}{D} = m\alpha \tag{2a}$$

$$\delta/c = \frac{b - \cos \alpha}{D} \tag{2b}$$

where

$$D = \left(b - \sqrt{b^2 - 1}\right) \sin \alpha + \frac{1}{\pi}\left[2 \cos \alpha + (b \cos \alpha - 1) \ln \frac{b-1}{b+1}\right]$$

This result is plotted as the variation of m with δ/c for various angles of attack in Fig. 2.

Although gravity is neglected in Green's solution, the forces on the plate can still be obtained in terms of δ/c from Eq. (2) if the Froude number V^2/gc is large. On the other hand, the relationship between the spray thickness and the actual leading edge depth of submersion cannot be determined from Green's two-dimensional analysis. However, in the practical case, at small angles of attack the depth of submersion and spray thickness may be taken as identical even at relatively shallow depths. From Fig. 2 it may be seen that for depths greater than about 1 chord the depth and spray thickness may be considerably different without affecting the value of m. Thus at depths greater than about 1 chord the assumption that $d/c = \delta/c$ is adequate in determining the forces. However at large angles of attack and shallow depths a better relationship is needed between d/c and δ/c if adequate accuracy is to be maintained. No theoretical solution for the relationship has been obtained. However, to give an idea of the relationship between these variables, experimentally obtained lines of constant d/c for an aspect ratio-1 flat plate are shown in Fig. 2. Experience has shown that these lines are sufficiently accurate for determining the value of m for moderate aspect ratios. The lines of constant d/c were faired to a value of $\alpha = 90$ degrees obtained from the equation

$$\delta/c = d/c + f/c \tag{3}$$

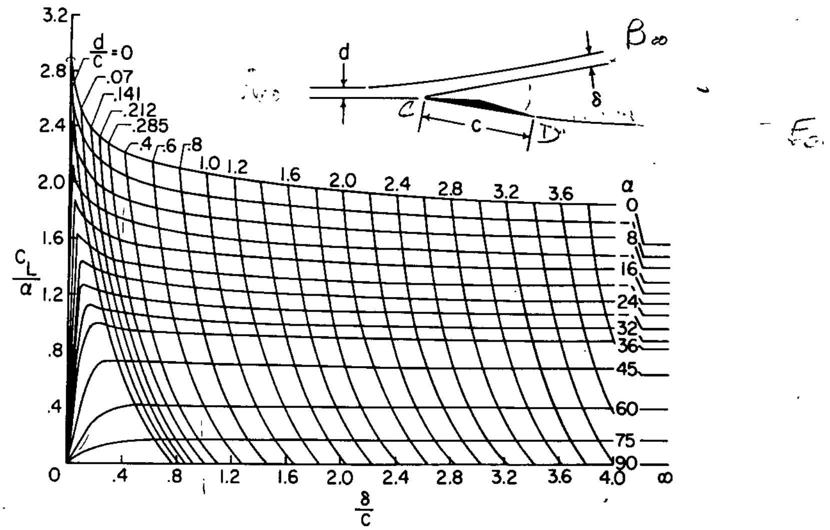

Fig. 2 - Green's solution for the lift-curve slope of a two-dimensional flat plate (with approximate lines of constant d/c)

where f/c is the dimensionless distance from the leading edge to the stagnation line. The distance f/c can be obtained from Green's work and for α = 90 degrees is

$$\frac{f}{c} = \frac{1 + \frac{\pi b}{2} + \ln\left(\frac{b}{b-1}\right) - \sqrt{b^2 - 1}\left(\frac{\pi}{2} \sin^{-1}\frac{1}{b}\right)}{\pi(b - \sqrt{b^2 - 1}) + \ln\left(\frac{b+1}{b-1}\right)} \tag{4}$$

where b has been previously defined in Eq. (2). Equation (3) is based on the assumption that the stagnation line for the condition α = 90 degrees is parallel to the undisturbed water surface.

Linearized Solution for Cambered Sections at Infinite Depth—The case of cambered surfaces at infinite depth can theoretically be analyzed in two dimensions by the method of Levi-Civita (10). However, like many conformal mapping problems the method is very difficult to apply to a particular configuration and only a few specific solutions have been obtained. Among these is the work of Rosenhead (11) and Wu (12). Although the solution of Wu is applicable in principle to arbitrary sections, it has been carried out only for the circular arc. A particular advantage of Wu's solution is that it includes the effects of nonzero cavitation number.

The most useful treatment of cambered surfaces is the linearized theory of Tulin and Burkart (1) which is readily applicable to any surface configuration (with positive lower surface pressures) as long as the angle of attack and camber are small. The principal results of this linearized theory are summarized below.

The supercavitating hydrofoil problem in the z plane is transformed into an airfoil problem in the $\bar{z}$ plane by the relationship $z = -\sqrt{\bar{z}}$. Denoting properties of the equivalent airfoil with barred symbols and those of the hydrofoil with unbarred symbols, the following relationships are derived:

$$\frac{d\bar{y}}{d\bar{x}}(\bar{x}) = \frac{dy}{dx}(\bar{x}^2) \tag{5}$$

$$\bar{u}(\bar{x}) = u(\bar{x}^2) \tag{6}$$

$$C_L = \bar{C}_m = \frac{\pi}{2}\left(A_o + A_1 - \frac{A_2}{2}\right) \tag{7}$$

$$C_D = 1/8\pi(\bar{C}_L^2) = \frac{\pi}{2}\left(A_o + \frac{A_1}{2}\right)^2 \tag{8}$$

$$C_m = \bar{C}_{m,3} = \frac{\pi}{32}(5A_o + 7A_1 - 7A_2 + 3A_3 - A_{4/2})\ . \tag{9}$$

The coefficients A_n are the thin airfoil coefficients in the sine series expansion of the airfoil vorticity distribution

$$\Omega(x) = 2V\left(A_o \cot\frac{\theta}{2} + \sum_{n=1}^{\infty} A_n \sin n\theta\right) \tag{10a}$$

where

$$x = \frac{1}{2}\bar{c}(1 - \cos\theta) \qquad (0 \leq \theta \leq \pi) \tag{10b}$$

and can be found for a given configuration from the following equations:

$$A_o = -\frac{1}{\pi}\int_0^{\pi} \frac{d\bar{y}}{d\bar{x}}\, d\theta + \alpha = \alpha + A_o' \tag{11a}$$

$$A_n = \frac{2}{\pi}\int_0^{\pi} \frac{d\bar{y}}{d\bar{x}} \cos n\theta\, d\theta\ . \tag{11b}$$

The first term in equation (10a), that is, the A_o term, is the vorticity due to angle of attack and the second term is that due to camber. In order to isolate the effects of camber, A_o will be considered zero. Any section profile derived on this basis will also, for convenience, be orientated with respect to the $\bar{X}$-axis in such a manner that $A_o' = 0$. From Eq. (9a) these conditions require that α also be equal to zero. Thus, the derived orientation is defined as the zero-angle-of-attack case.

When A_o is set equal to zero, the hydrofoil lift/drag ratio for a given lift coefficient is obtained from Eqs. (7) and (8) as follows:

$$\frac{C_L}{C_D} = \frac{\left(A_1 - \frac{A_2}{2}\right)^2}{A_1{}^2/4}\ \frac{\pi}{2C_L} = 4\left(1 - \frac{A_2}{2A_1}\right)^2 \frac{\pi}{2C_L}\ . \tag{12}$$

Obviously, for maximum lift/drag ratio, $-A_2/A_1$ must be as large as possible. However, if the assumed condition that a cavity exists only on the upper surface is to be real, the vorticity distribution given by Eq. (8) must be positive in the interval $0 \leq \theta \leq \pi$; that is, the pressure on the hydrofoil lower surface must be positive over the entire chord, otherwise a cavity will exist on the lower surface. Thus, for maximum hydrofoil lift/drag ratio, $-A_2/A_1$ must be as large as possible and still satisfy the condition

$$\Omega(\bar{x}) = 2V \sum_{n=1}^{\infty} A_n \sin n\theta \geqq 0 \qquad (0 \leqq \theta \leqq \pi) . \tag{13}$$

Tulin-Burkart Section—With the stipulation that the vorticity distribution is defined by only two terms in Eq. (13), Ref. 1 finds the optimum relationship between A_1 and A_2 as $-A_2/A_1 = 1/2$. This results in a hydrofoil configuration given by the equation

$$\frac{y}{c} = \frac{A_1}{2}\left[\left(\frac{x}{c}\right) + \frac{8}{3}\left(\frac{x}{c}\right)^{3/2} - 4\left(\frac{x}{c}\right)^2\right] . \tag{14}$$

From Eq. (7) the design lift coefficient (that is, for $\alpha = 0$) for this section is

$$C_{L,d} = \frac{5\pi A_1}{8} \tag{15}$$

and the lift/drag ratio for this condition as obtained from Eq. (12) is

$$\frac{L}{D} = \frac{25}{4}\left(\frac{\pi}{2C_L}\right) . \tag{16}$$

Since $\pi/2C_L$ represents the lift/drag ratio of a flat plate, the configuration given by Eq. (14) has a lift/drag ratio 25/4 times as great as that of the flat plate. When the hydrofoil given in Eq. (14) is operated at an angle of attack, the lift/drag ratio becomes

$$\frac{L}{D} = \frac{\alpha + \frac{2}{\pi} C_{L,d}}{\alpha + \frac{4}{5\pi}\left(C_{L,d}\right)^2} . \tag{17}$$

In Ref. 1 it is pointed out that configurations superior to the one given by Eq. (14) are possible. In Ref. 2 two such superior configurations are selected.

Three-Term Section—If the vorticity distribution given by Eq. (10) is assigned three terms, it is shown in Ref. 2 that the optimum vorticity distribution for low drag is

$$\Omega(\bar{x}) = 2V A_1 \left(\sin\theta - \sin 2\theta + \frac{1}{2}\sin 3\theta\right) . \tag{18}$$

The shape of the hydrofoil corresponding to Eq. (18) is

$$\frac{y}{c} = \frac{A_1}{10}\left[5\left(\frac{x}{c}\right) - 20\left(\frac{x}{c}\right)^{3/2} + 80\left(\frac{x}{c}\right)^2 - 64\left(\frac{x}{c}\right)^{5/2}\right] . \tag{19}$$

By using Eq. (7), the lift coefficient of this hydrofoil becomes

$$C_L = \frac{\pi}{2}\left(\alpha + \frac{3A_1}{2}\right) \tag{20}$$

or for $\alpha = 0$ the design lift coefficient is

$$C_{L,d} = \frac{3\pi A_1}{4} . \tag{21}$$

The following drag coefficient may be obtained by using Eq. (8):

$$C_D = \frac{\pi}{2}\left(\alpha + \frac{A_1}{2}\right)^2 = \frac{\pi}{2}\left(\alpha + \frac{2C_{L,d}}{3\pi}\right)^2 . \tag{22}$$

For $\alpha = 0$, the lift/drag ratio is

$$\frac{L}{D} = 9\left(\frac{\pi}{2C_L}\right) . \tag{23}$$

This value is nine times as large as that for a flat plate and 1.44 times as large as the value for the hydrofoil of Ref. 1 where $L/D = 25/4\,(\pi/2C_L)$. The following lift/drag ratio may be obtained for finite angles of attack by dividing Eq. (20) by Eq. (22)

$$\frac{L}{D} = \frac{\alpha + \frac{2}{\pi} C_{L,d}}{\left(\alpha + \frac{2C_{L,d}}{3\pi}\right)^2} . \tag{24}$$

Five-Term Section—Another hydrofoil section which theoretically has lower drag than either of the previously discussed profiles can be obtained by assigning the following value to Eq. (10)

$$\Omega(\bar{x}) = 2V A_1 (\sin\theta - 4/3 \sin 2\theta + 4/3 \sin 3\theta - 2/3 \sin 4\theta + 1/3 \sin 5\theta) . \tag{25}$$

The shape of the hydrofoil corresponding to Eq. (25) is

$$\frac{y}{c} = \frac{A_1}{315}\left[210\left(\frac{x}{c}\right) - 2,240\left(\frac{x}{c}\right)^{3/2} + 12,600\left(\frac{x}{c}\right)^2 - 30,912\left(\frac{x}{c}\right)^{5/2} + 35,840\left(\frac{x}{c}\right)^3 - 15,360\left(\frac{x}{c}\right)^{7/2}\right] . \tag{26}$$

By using Eq. (7), the lift coefficient of this hydrofoil may be given as

$$C_L = \frac{\pi}{2}\left(\alpha + \frac{5A_1}{3}\right) \tag{27}$$

or for $\alpha = 0$ the design lift coefficient is

$$C_{L,d} = \frac{5\pi A_1}{6} . \tag{28}$$

The following drag coefficient is obtained by using Eq. (8):

$$C_D = \frac{\pi}{2}\left(\alpha + \frac{A_1}{2}\right)^2 = \frac{\pi}{2}\left(\alpha + \frac{3C_{L,d}}{5}\right)^2 \tag{29}$$

and for $\alpha = 0$ the lift/drag ratio is

$$\frac{L}{D} = \frac{100}{9}\left(\frac{\pi}{2C_L}\right) . \tag{30}$$

This lift/drag ratio is about 11 times as large as the value for a flat plate and nearly twice as efficient as the configuration of Ref. 1.

For finite angles of attack,

$$\frac{L}{D} = \frac{\alpha + \frac{2}{\pi} C_{L,d}}{\left(\alpha + \frac{3}{5\pi} C_{L,d}\right)^2} . \tag{31}$$

Circular-Arc Section—Because of the geometrical simplicity of the circular-arc profile, it is desirable to include its characteristics so that the circular arc may be compared with the other low-drag sections. Denoting the central angle subtending the chord as γ and using the chord line as the reference axis, the coefficients for the circular arc determined from the linearized theory are

$$A_o' = -\frac{\gamma}{8} \tag{32a}$$

$$A_1 = \frac{\gamma}{2} \tag{32b}$$

$$A_2 = -\frac{\gamma}{8} \tag{32c}$$

$$A_n = 0 \qquad (n > 2). \tag{32d}$$

Since for the reference axis used, A_o' is negative, positive lower-surface pressures cannot possibly be realized near the leading edge unless the angle of attack is increased at least to the point where $\alpha - \gamma/8 = 0$. Because $A_n = 0$ for $\eta > 2$ and $A_1 \sin\theta + A_2 \sin 2\theta$ is everywhere positive in the interval $0 \leqq \theta \leqq \pi$, the condition $\alpha - \gamma/8 = 0$ is sufficient to specify positive pressures over the entire chord of the hydrofoil. A convenient way of treating the circular-arc section to make it comparable to the other low-drag sections is to reorient its reference line an angle $\gamma/8$ above the chord line so that for this orientation $A_o' = 0$ and $\alpha = 0$. Using this new reference line the lift coefficient of the circular-arc section is

$$C_L = \frac{\pi}{2} \left(\alpha + \frac{9}{16}\right)\gamma \tag{33}$$

or for $\alpha = 0$ the design lift coefficient is

$$C_{L,d} = \frac{9\pi}{32} \gamma . \tag{34}$$

The following drag coefficient is obtained by using Eqs. (8) and (34):

$$C_D = \frac{\pi}{2} \left(\alpha + \frac{\gamma}{4}\right)^2 = \frac{\pi}{2} \left(\alpha + \frac{8}{9\pi} C_{L,d}\right)^2 \tag{35}$$

and for $\alpha = 0$ the lift/drag ratio is

$$\frac{L}{D} = \frac{81}{16} \frac{\pi}{2C_L} . \tag{36}$$

This lift/drag ratio is about 5 times as large as the value for a flat plate and almost as great as the Tulin-Burkart section.

For finite angles of attack

$$\frac{L}{D} = \frac{\alpha + \frac{2}{\pi} C_{L,d}}{\left(\alpha + \frac{8}{9\pi} C_{L,d}\right)^2} . \tag{37}$$

Comparison of Sections—The shape of the four sections discussed in the preceding paragraphs are shown for comparison in Fig. 3a. The pressure distribution on these sections is presented in Fig. 3b. It may be noted that the location of maximum pressure moves rearward with increase in the ratio $-A_2/A_1$.

The lift/drag ratio given by Eqs. (17), (24), (31), and (37) are compared in Fig. 4. The great improvement over the L/D of a flat plate offered by positively cambering the lower surface and operating at the design angle of attack is most encouraging. However, a comparison at what amounts to a fictional design angle of attack is not justified. It is obvious from a structural standpoint that hydrofoils with any strength must be operated at finite angles of attack (corresponding to the dashed lines in Fig. 4). Thus the maximum lift/drag ratio for any section depends on the minimum angle at which it can be operated with a cavity from the leading edge. A meaningful comparison of the hydrofoil sections just discussed is not possible unless the influence of the upper surface of the hydrofoil is also included, for it is this surface which controls the maximum lift/drag ratio of the section. Assuming infinite speed and thus zero cavitation number, it is clear that if any portion of the upper surface becomes wetted, the lift will decrease and the drag increase. Thus, a knowledge of the profile of the given hydrofoil upper surface combined with the location of the upper cavity streamline at various angles of attack will permit the prediction of the angle of attack at which the maximum lift/drag ratio will occur. Only on the basis of maximum lift/drag ratio can the best supercavitating hydrofoil be selected. A comparison of the various sections based on calculated cavity streamline locations and hydrofoil thickness is presented in the last section of this paper.

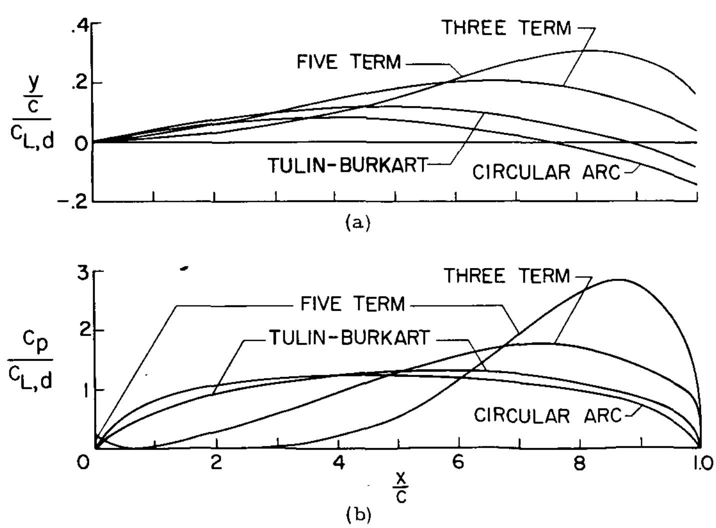

Fig. 3 - Shape and pressure distribution of four low-drag supercavitating hydrofoils; $\alpha = 0$; infinite depth: (a) lower surface profile, (b) pressure distribution

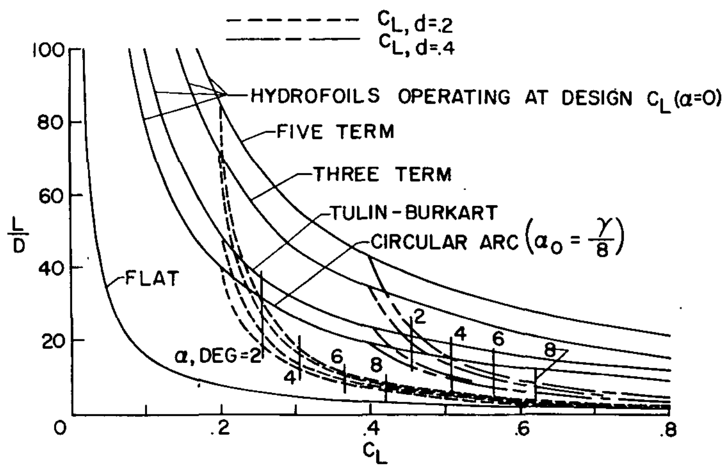

Fig. 4 - Lift/drag ratios for low-drag hydrofoils calculated from two-dimensional linearized theory

The practical use of the formulas presented in the preceding discussion is also limited by the assumptions made in their derivation. In fact, the restrictions imposed by the assumptions of the linearized theory prevent its use in the calculation of the characteristics of hydrofoils suitable for use as aircraft landing gear. Here, because of the high hydrofoil loads on necessarily thin hydrofoils the aspect ratio may be as low as 1 or 2. Also the hydrofoil must operate near the free water surface and in some instances at large angles of attack. Thus, the effects of these variables on the characteristics of supercavitating hydrofoils (particularly of cambered sections) is needed. Much of this information can be obtained by additional application of the linearized theory combined with certain modifications to the two-dimensional theory discussed in preceding paragraphs.

Modifications of Infinite Depth Theory

Nonlinear Equation for Lift at Infinite Depth—If $\alpha = 0$ refers to the reference line which makes $A_0' = 0$, then Eq. (7) may be written as

$$C_L = \frac{\pi}{2}\left(\alpha + A_1 - \frac{A_2}{2}\right) = \frac{\pi}{2}(\alpha + \alpha_c) \tag{38}$$

where α_c is the effective increase in angle of attack due to camber $(A_1 - A_2/2)$. Thus, the solution for cambered hydrofoils is merely the flat-plate linearized solution $\pi\alpha/2$ with α replaced by $\alpha + \alpha_c$. This is exactly analogous to the influence of camber on airfoils in an infinite fluid where there is an effective increase in angle of attack due to the camber. By carrying this procedure further, and by applying it to the resultant force rather than the lift, the nonlinear solution of Rayleigh becomes applicable to arbitrary configurations simply by replacing α by $\alpha + \alpha_c$; that is,

$$C_N \cong \frac{2\pi \sin(\alpha + \alpha_c)}{4 + \pi \sin(\alpha + \alpha_c)} \,. \tag{39}$$

The lift will then be

$$C_L \cong \frac{2\pi \sin(\alpha + \alpha_c)}{4 + \pi \sin(\alpha + \alpha_c)} \cos \beta . \tag{40}$$

In Eq. (40), $\beta = \alpha + \epsilon$, where ϵ denotes the deviation of the resultant-force vector from the normal to the hydrofoil reference line. For large values of α, ϵ is small compared with α and $\cos \beta \cong \cos \alpha$. When α is very small, ϵ is a maximum and will almost always be less than about 3 degrees, for which the cosine is very nearly 1 or cosine $(\alpha + \epsilon) \cong \cos \alpha \cong 1$. Therefore, $\cos \beta$ in equation (38) may be replaced by $\cos \alpha$ with little lose in accuracy and great gain in simplicity. Equation (40) then becomes

$$C_L \cong \frac{2\pi \sin(\alpha + \alpha_c)}{4 + \pi \sin(\alpha + \alpha_c)} \cos \alpha . \tag{41}$$

For a circular-arc hydrofoil of central angle γ, it has been shown in Eq. (33) that $\alpha_c = (9/16)\ \gamma$. It has also been shown that for the circular arc the reference line must be chosen at an angle $\gamma/8$ to the chord line so that $A_0' = 0$. The result obtained by substituting $\alpha_c = (9/16)\ \gamma$ into Eq. (41) is compared in Fig. 5 with the linear solution of Tulin and Burkart (Eq. 38) and the nonlinear solution of Wu (12) for two circular-arc profiles. The agreement of Eq. (39) with the more exact solution of Wu is good over the entire range of angle of attack from 0 to 90 degrees. Similar agreement is expected for any configuration of small camber.

The successful modification of the Rayleigh equation to include cambered configurations leads at once to a similar modification of the solution of Green. However, in this case the argument for replacing α by $\alpha + \alpha_c$ is very weak unless the section coefficients which determine α_c are known as a function of the depth of submersion.

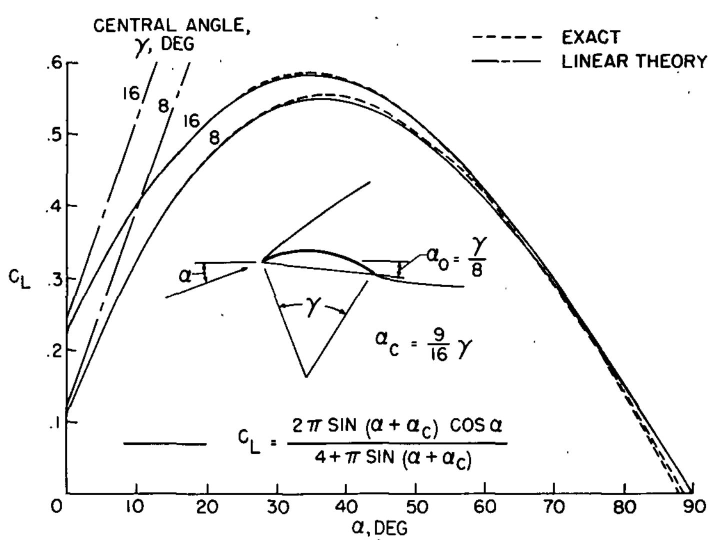

Fig. 5 - Two-dimensional theories for the lift coefficient of a circular-arc hydrofoil at infinite depth

Linearized Solution for Lift of Cambered Sections at Finite Depth—An examination of the linearized expressions for the lift coefficient of arbitrary foils at infinite depth and at zero depth reveals that both the lift-curve slope and the increase in angle of attack due to camber do change with depth of submersion. At infinite depth the linearized expression for lift coefficient is given by Eq. (33). At zero depth the lift coefficient must be one-half the fully wetted value obtained from thin-airfoil theory as pointed out in Ref. 13; that is,

$$C_{L,0} = \pi \left(A_{0,h} + \frac{A_{1,h}}{2}\right) \tag{42}$$

where $A_{0,h}$ and $A_{1,h}$ are the thin-airfoil coefficients of the section in the hydrofoil plane and are given by the expressions

$$A_{0,h} = -\frac{1}{\pi}\int_0^\pi \frac{dy}{dx}\, d\theta \tag{43a}$$

$$A_{1,h} = \frac{2}{\pi}\int_0^\pi \frac{dy}{dx} \cos\theta\, d\theta\,. \tag{43b}$$

For the Tulin-Burkart section at zero angle of attack these values may be determined as

$$A_{0,h} = 0.227\ A_1 \tag{44a}$$

$$A_{1,h} = 1.151\ A_1\,. \tag{44b}$$

Thus, from Eqs. (38) and (42) it is seen that, for a flat plate at small angles, the lift coefficient goes from $\pi\alpha/2$ at infinite depth to $\pi\alpha$ at zero depth (as given by Green), whereas for the Tulin-Burkart section at zero angle of attack these values are $\pi(1.25\ A_1)/2$ at infinite depth and $\pi(0.802\ A_1)$ at zero depth. Although the flat-plate lift coefficient doubles in going from infinite to zero depth, the ratio is only 1.28 for the cambered section. The important point to note is that the value of α_c for the Tulin-Burkart section changes from $1.25\ A_1$ to $0.802\ A_1$.

It is now desirable to determine α_c for finite depths of submersion. This can be accomplished by modifying the linearized theory of Ref. 1 to include the effects of the free water surface.

Rigorous Solution—The effect of the free water surface may be obtained by finding the transformation which will map the free water surface, the hydrofoil, and the cavity streamlines into the real axis of an auxiliary or equivalent airfoil plane denoted as the ζ plane to distinguish from the $\bar{Z}$ plane used at infinite depth. The transformation required is

$$Z = \frac{d}{\pi}\left(\zeta - \ln\zeta - 1\right) \tag{45}$$

where d is the depth of submersion of the leading edge, or more exactly the spray thickness δ. The Z plane and its transformation in the ζ plane are shown in Fig. 6. In the linearized theory developed in Ref. 1 points of corresponding perturbation velocities u and v remain constant in the transformation; therefore, the boundary conditions shown in the Z plane are shown in the ζ plane in their corresponding locations. The potential flow problem shown in the ζ plane is exactly the thin airfoil

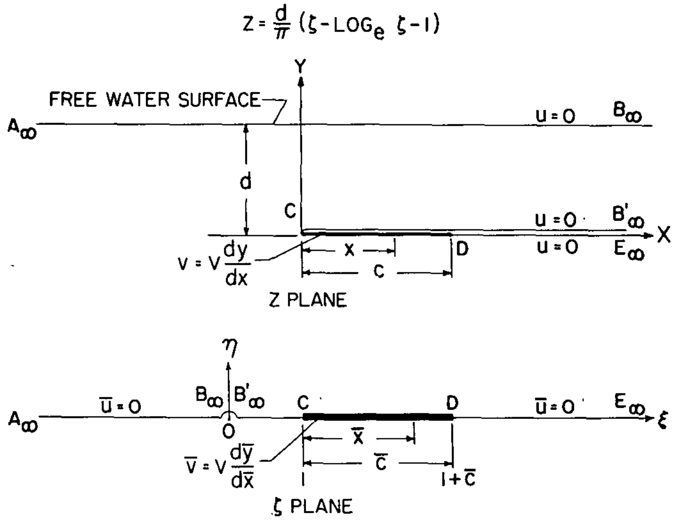

Fig. 6 - Transformation of hydrofoil at finite depth to equivalent airfoil

problem. It is well known that the thin airfoil problem can be solved by distributing vortices along the chord so that the condition $\bar{v} = (d\bar{y}/d\bar{x})V$ is satisfied (14). The desired distribution of vorticity is $\Omega(\bar{x})$ as given in Eq. (8). With $\Omega(\bar{x})$ known, $\bar{u}(\bar{x})$ and $\bar{v}(\bar{x})$ are known. These values of $\bar{u}$ and $\bar{v}$ on the airfoil are exactly the same as the values of u and v on the hydrofoil if the relationship between x and $\bar{x}$ satisfies the equation

$$x = \frac{d}{\pi}\left[\bar{x} - \ln(1 + \bar{x})\right]. \tag{46}$$

Equation (46) is obtained directly from Eq. (45) by noting that $\zeta = 1 + \bar{x}$. Dividing Eq. (46) through by c gives

$$\frac{x}{c} = \frac{1}{\pi}\,\frac{d}{c}\,[\bar{x} - \ln(1 + \bar{x})]\,. \tag{47}$$

When $\frac{x}{c} = 1$, $\bar{x} = \bar{c}$, therefore

$$\frac{d}{c} = \frac{\pi}{\bar{c} - \ln(1 + \bar{c})}\,. \tag{48}$$

Using Eqs. (47) and (48) the relationship between x/c and $\bar{x}/\bar{c}$ may be determined for both positive and negative values of $\bar{x}/\bar{c}$. It can be seen in Fig. 6b that negative values of $\bar{x}/\bar{c}$ correspond to points in front of the airfoil which in turn are related to points on the upper cavity streamline. The relationship between $\bar{x}/\bar{c}$ and x/c is presented in Fig. 7. With the aid of Fig. 7 and a knowledge of thin-airfoil theory the solution to the supercavitating hydrofoil problem at finite depth is easily determined. The word easily refers to the comprehension of the solution; the actual labor is considerably involved because of the necessity to frequently resort to plotting curves and employing a planimeter.

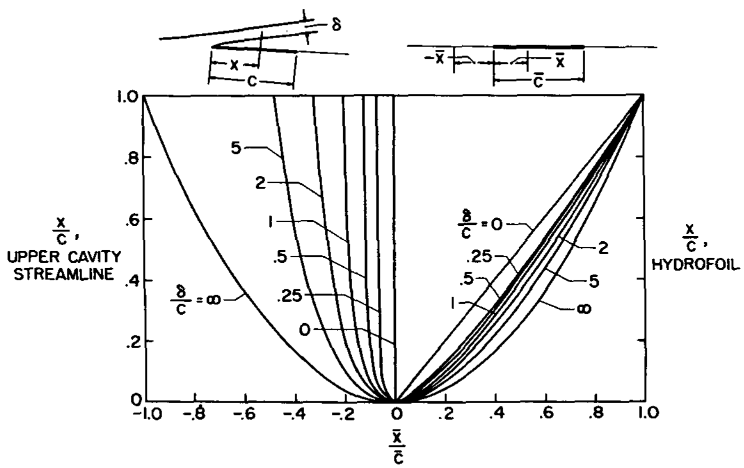

Fig. 7 - The influence of depth of submersion on the relationship between points in hydrofoil and equivalent airfoil planes

The procedure for determining the pressure distribution and thus the forces and moments on a hydrofoil at arbitrary depth is as follows:

1. The shape of the hydrofoil is known as $y = y(x)$ and thus

$$\frac{dy}{dx} = \frac{dy}{dx}(x) \quad \text{or} \quad \frac{dy}{dx}\left(\frac{x}{c}\right).$$

2. The slope of the equivalent airfoil at the point $\bar{x}/\bar{c}$ is exactly the same as the slope of the hydrofoil $dy/dx(x/c)$ when x/c and $\bar{x}/\bar{c}$ are related as shown in Fig. 7. Thus $dy/d\bar{x}(\bar{x}/\bar{c})$ is found.

3. The vorticity distribution on the airfoil is then obtained from Eqs. (8) and (9).

4. The perturbation velocity $\bar{u}$ in terms of the vorticity Ω is given by the equation

$$\bar{u}\left(\frac{\bar{x}}{\bar{c}}\right) = \frac{1}{2}\Omega\left(\frac{\bar{x}}{\bar{c}}\right) \tag{49}$$

Thus the velocity $\bar{u}(\bar{x}/\bar{c})$ is determined at every point along the airfoil.

5. The perturbation velocity $u(x/c)$ on the hydrofoil is exactly the same as the velocity $\bar{u}(\bar{x}/\bar{c})$ if $\bar{x}/\bar{c}$ and x/c are related as shown in Fig. 7. Thus the velocity $u(x/c)$ is determined.

6. Step 5 also determines the linearized pressure coefficient since C_p is given by the equation

$$C_p = \frac{p - p_\infty}{q} = 2\,\frac{u}{V}$$

or

$$C_p\left(\frac{x}{c}\right) = A_o' \cot\frac{\theta}{2} + \sum A_n \sin n\theta \tag{50}$$

where θ is related to x/c by Eq. (10b) and Fig. 7.

7. With a knowledge of $C_p(x/c)$ the lift, drag, and moment coefficients are determined as

$$C_L = \int_0^1 C_p\left(\frac{x}{c}\right) d\frac{x}{c} \tag{51a}$$

$$C_D = \int_0^1 C_p\left(\frac{x}{c}\right)\frac{dy}{dx}\, d\frac{x}{c} \tag{51b}$$

$$C_m = \int_0^1 C_p\left(\frac{x}{c}\right)\frac{x}{c}\, d\frac{x}{c}\ . \tag{51c}$$

Approximate Solution—The calculations by the rigorous method outlined above were so cumbersome that the solution by this method was abandoned when an approximate method was discovered. The approximate method continues with the simple transformation $\overline{Z} = -\sqrt{\overline{Z}}$ used in Ref. 1. The advantage of the simpler transformation is that if the vorticity distribution in the presence of the water surface can be determined in the $\overline{Z}$ plane, the simple Eqs. (7) and (9) for the lift and moment coefficient will still be applicable. It is shown in Ref. 3 that the influence of the free surface on the equivalent airfoil in the $\overline{Z}$ plane can be approximated by locating a singular vortex in the position shown in Fig. 8. The strength of this vortex Γ_i is equivalent to the total circulation about the airfoil. Using the model shown in Fig. 8 and equating

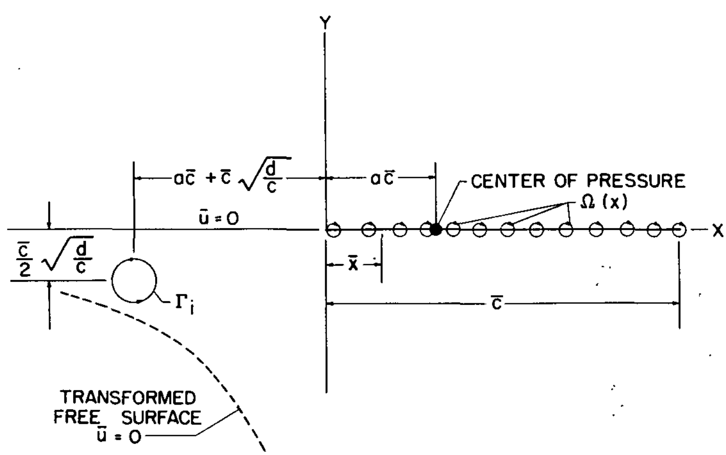

Fig. 8 - Linearized model for calculating the effect of depth of submersion on the vorticity distribution of the equivalent airfoil section using the $Z = -\sqrt{\overline{Z}}$ transformation

the airfoil slope at the point $\bar{x}$ to the streamline slopes induced by the sum of the airfoil vorticity and the image vortex; the airfoil vorticity was determined in Ref. 3 as

$$\Omega(\bar{x}) = 2V\left(C_o \cot\frac{\theta}{2} + \sum_{n=1}^{\infty} C_n \sin n\theta\right) \tag{52}$$

where

$$C_o = \frac{A_o(4 + B_1) + A_1 B_o}{4 + B_1 - 2B_o} \tag{53a}$$

$$C_1 = \frac{2A_1(2 - B_o) - 2A_o B_1}{4 + B_1 - 2B_o} \tag{53b}$$

$$C_n = A_n - \frac{(2A_o + A_1)B_n}{4 + B_1 - 2B_o}. \tag{53c}$$

The B coefficients are given in Fig. 9 in terms of the center of pressure location $a\bar{c}$ where a is given by the equation

$$a = \frac{1}{4}\,\frac{C_o + C_1 - \frac{C_2}{2}}{C_o + \frac{C_1}{2}}. \tag{54}$$

The A coefficients (Eqs. 53) are the section coefficients for infinite depth.

The C coefficients are computed by iteration; that is, a value of a is assumed, the B coefficients are obtained from Fig. 9, and the C coefficients determined from Eqs. (53). If the value of a determined from Eq. (54) does not agree with the original assumption, the procedure should be repeated.

If the C coefficients are determined for the case of α or $A_o = 0$, the ratio of the lift coefficient due to camber at finite depth to the lift coefficient due to camber at infinite depth may be determined from the following equation:

$$\left(\frac{C_L}{C_{L,\infty}}\right)_{\alpha=0} = \frac{C_o + C_1 - \frac{C_2}{2}}{A_1 - \frac{A_2}{2}}. \tag{55}$$

The values of $(C_L/C_{L,\infty})_{\alpha=0}$ given by Eq. (55) for the four sections of interest are presented in Fig. 10.

The true linearized lift-curve slope m for finite depths of submersion in the equation $C_L = m_{(\alpha + \alpha_c)}$ is that shown in Fig. 2 for $\alpha = 0$. Therefore, the effective angle of attack due to camber α_c is obtained from the following relationship:

$$\frac{m_{(\alpha=0)}\alpha_c}{\frac{\pi}{2}\alpha_{c,\infty}} = \left(\frac{C_L}{C_{L,\infty}}\right)_{\alpha=0}. \tag{56}$$

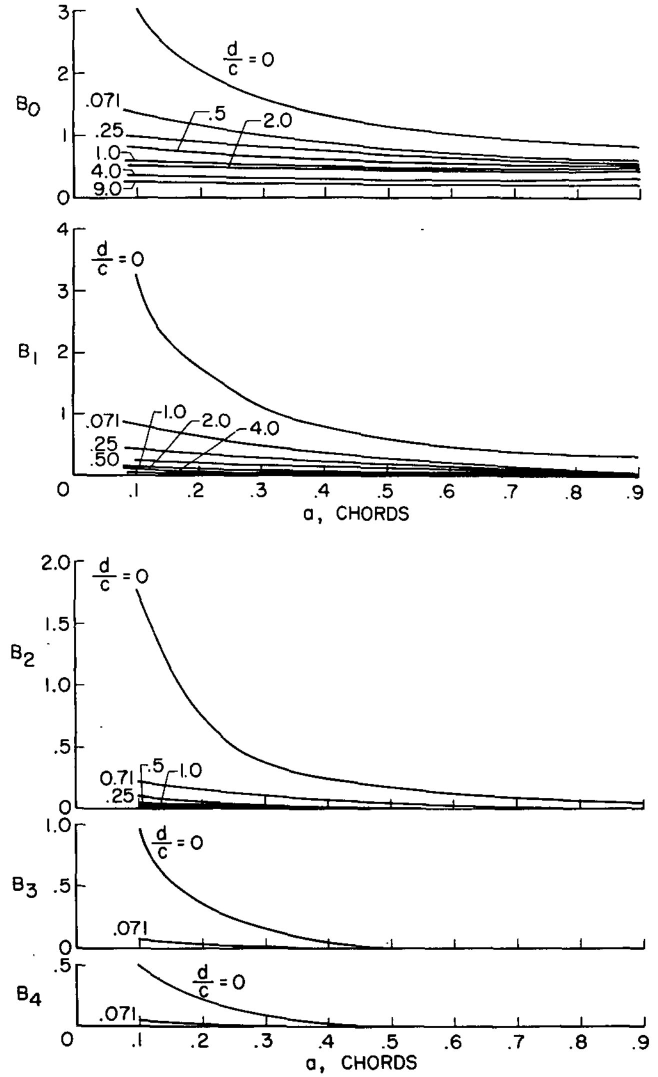

Fig. 9 - The B coefficients (a) B_0 and B_1, (b) B_2, B_3, and B_4

Thus

$$\frac{\alpha_c}{\alpha_{c,\infty}} = \frac{\pi}{2m_{(\alpha=0)}} \frac{C_L}{C_{L,\infty}}.$$

Values of $\alpha_c/\alpha_{c,\infty}$ are plotted against d/c in Fig. 11 for the Tulin-Burkart, the circular-arc, and the three-term and five-term sections.

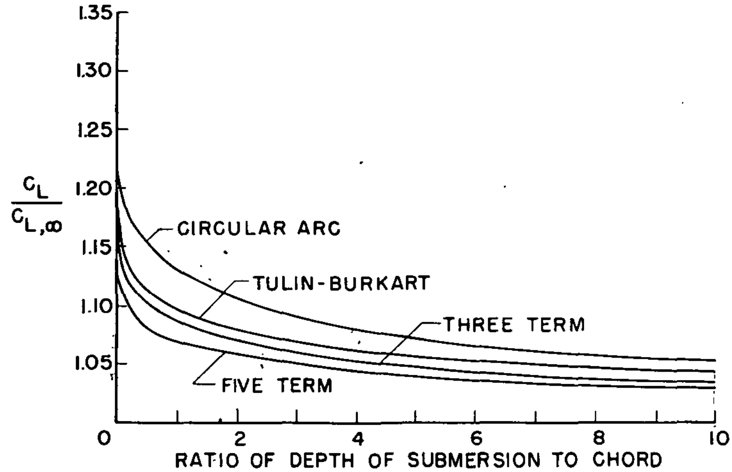

Fig. 10 - Influence of depth of submersion on the lift coefficient of cambered sections operating at the design angle of attack ($\alpha = 0$).

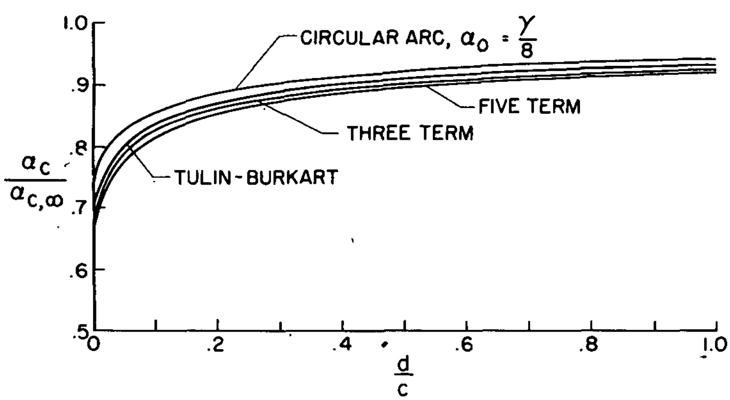

Fig. 11 - Influence of depth of submersion on the effective angle of attack α of cambered sections operating at the design angle of attack ($\alpha = 0$)

Equation (57) is obviously limited by the linearizing assumptions made in its derivation. An important limitation is due to the assumption that the free surface is always horizontal and thus $\delta/c = d/c$. At small depth/chord ratios and particularly for large magnitudes of camber the free water surface is not horizontal and $\delta/c \neq d/c$. Thus, for small values of d/c and large magnitudes of camber the values of $\alpha_c/\alpha_{c,\infty}$ given in Fig. 11 are probably too low.

Nonlinear Equation for Lift at Finite Depth—With a knowledge of the angle of attack due to camber α_c at finite depths of submersion, Green's solution is now modified to include camber by treating the effective angle of attack as $\alpha + \alpha_c$, where α_c is obtained from Fig. 11. This is exactly the method used in modifying the Rayleigh equation to obtain the nonlinear approximation for the lift coefficient at infinite depth. With this assumption, the resultant-force coefficient for a cambered hydrofoil at any positive depth of submersion is obtained in terms of the spray thickness δ/c from Eqs. (2) as

$$C_N\{\alpha\} = C_{N,f}\{\alpha + \alpha_c\} . \tag{58}$$

Equation (58) states that the resultant force on a cambered section is approximated by replacing α in Green's solution for a flat plate by the effective angle of attack $\alpha + \alpha_c$. It will be shown that the resultant force will deviate only slightly from the normal (as previously pointed out for the condition of infinite depth) and therefore

$$C_L\{\alpha\} = C_{N,f}\{\alpha + \alpha_c\} \cos \alpha . \tag{59}$$

Three-Dimensional Theory at Finite Depth—Lift—The flow about a supercavitating hydrofoil may be constructed by a suitable combination of sources and vortices. The vortices contribute unsymmetrical velocity components and lift; the sources contribute symmetrical components which provide thickness for the cavity but no lift. For a finite span the vortices cannot end at the tips of the foil, and a system of horseshoe vortices must be combined with the sources to describe the flow. If it is assumed that the influence of finite span on the two-dimensional lift coefficient is due to the effects of the trailing vorticity, then the resulting effect of aspect ratio is exactly the same as for a fully wetted airfoil. Jones (15) gives the lift of a fully wetted elliptical flat plate as

$$\bar{C}_L = \frac{1}{E} 2\pi(\alpha - \alpha_i) \tag{60}$$

where E is the ratio of semiperimeter to the span and α_i is the induced angle of attack caused by the trailing vorticity. Thus the effect of aspect ratio is to decrease the two-dimensional lift curve slope by a factor $1/E$ and to decrease the effective angle of attack by an increment α_i. Therefore for the finite aspect ratio supercavitating hydrofoil at infinite depth Eq. (38) is modified to give

$$C_{L,1} = \frac{1}{E} \frac{\pi}{2} (\alpha + \alpha_c - \alpha_i) \tag{61}$$

or more generally for finite depth, Eq. (59) becomes

$$C_{L,1} \cong \frac{1}{E} C_{N,f}\{\alpha + \alpha_c - \alpha_i\} \cos \alpha \tag{62}$$

where for rectangular plan form of aspect ratio $A, E = (A + 1)/A$ and

$$\alpha_i = \frac{C_{L,1}}{\pi A} (1 + \tau) \tag{63}$$

where τ is a correction for plan form (see Ref. 14).

Another effect due to finite aspect ratio is the concept of additional lift due to crossflow (5,16). This crossflow lift is assumed due to the drag on the hydrofoil contributed by the component of free-stream velocity normal to the hydrofoil. In the present case of zero cavitation number, the crossflow drag coefficient is the Rayleigh value, 0.88. Since this lift is caused only by the spanwise flow (flow around the ends of the plate) it is also modified to account for the aspect ratio by the Jones' edge correction, $1/E$. Since only the spanwise flow is considered, E is now the ratio of semiperimeter to chord. Because the flow being considered is normal to the plate, the induced angle for this flow is zero. Thus for a flat plate, the crossflow lift $C_{L,c}$ is

$$C_{L,c} = \frac{1}{A+1} 0.88 \sin^2\alpha \cos\alpha . \tag{64}$$

No experimental or theoretical information on the crossflow lift of cambered surfaces is available in the literature. In order to approximate this component the following assumptions are made: (a) the crossflow force acts normal to the hydrofoil chord line, and (b) the effective direction of the free stream on the plate is altered by the increase in angle of attack due to camber α_c. Thus, the crossflow lift on cambered sections is assumed to be

$$C_{L,c} \cong \frac{1}{A+1} 0.88 \sin^2(\alpha' + \alpha_c) \cos\alpha' \tag{65}$$

where $\alpha' = \alpha + \alpha_o$, in which α_o is the inclination of the chord line to the reference line of the section (positive if the chord line is below the reference line), and α_c is obtained from Fig. 11 for the depth of interest.

The total lift on a finite aspect ratio hydrofoil operating near the free water surface is therefore obtained by adding Eq. (65) to Eq. (62) to give

$$C_L\{\alpha\} \cong \frac{A}{A+1} C_{n,f}\{\alpha + \alpha_c - \alpha_i\} \cos\alpha' + \frac{1}{A+1} 0.88 \sin^2(\alpha' + \alpha_c) \cos\alpha' . \tag{66}$$

In view of the very approximate nature of Eq. (65) it is desirable to examine the effect of this crossflow term on the total-lift coefficient. For a Tulin-Burkart, aspect-ratio-1 section ($A_1 = 0.2$) operating at $d/c = 0.071$ the ratio of the calculated crossflow lift, $C_{L,c}$ to the calculated total lift was 0.157 at $\alpha = 4$ degrees and 0.283 at $\alpha =$ 20 degrees. For a five-term section with $A_1 = 0.075$, aspect ratio = 3, and $d/c = 0.071$, the ratio has been calculated at 0.014 at $\alpha = 4$ degrees and 0.072 at $\alpha = 20$ degrees. Thus any inaccuracies in the crossflow lift as computed by Eq. (65) will appreciably affect the total-lift coefficient at large angles, small aspect ratios, and large cambers. On the other hand at higher aspect ratios and small cambers, errors in the crossflow component do not greatly influence the total calculated lift.

Equation (66) may be written in terms of the slope m (given in Fig. 2) as

$$C_L = \frac{A}{A+1} m(\alpha + \alpha_c - \alpha_i) \frac{\cos\alpha}{\cos(\alpha + \alpha_c - \alpha_i)} + \frac{1}{A+1} 0.88 \sin^2(\alpha' + \alpha_c) \cos\alpha' \tag{67}$$

where α_c is obtained from Fig. 11 for the depth-chord ratio of interest and α_i is obtained from Eq. (63). In Eq. (63) $C_{L,1}$ is the first term in Eq. (67). Equation (67) is solved by iteration and the convergence is quite rapid.

Drag—The drag coefficient of a supercavitating hydrofoil of finite aspect ratio operating at zero cavitation number and finite depth of submersion is

$$C_D = C_{L,1} \tan(\alpha + \epsilon) + C_{L,c} \tan\alpha' + C_f \tag{68}$$

where $C_{L,1}$ is the first term in Eq. (67) and ϵ is the deviation of the resultant-force vector from the normal. For a flat plate $\epsilon = 0$, $\alpha' = \alpha$, and thus $C_D = C_L \tan\alpha + C_f$. For cambered surfaces similar to the circular-arc or Tulin-Burkart section, ϵ becomes very small at large angles of attack and may be neglected; however, at small angles of attack, the effect of ϵ on the drag coefficient cannot be neglected. An approximation to the value of ϵ can be made by determining its value from the two-dimensional linearized solution and then modifying the result for the case of finite angles of attack and aspect ratio. Either the rigorous or approximate methods of obtaining the linearized drag coefficient may be used. Using the approximate method of determining the influence of the free water surface on the equivalent airfoil in the $\bar{z}$ plane, it is shown in Ref. 3 that the value of ϵ may be determined from the following equation:

$$\epsilon = \frac{(C_1 - 2C_2)\,A_1 + (2C_o + 2C_1 + C_4)\,A_2 - A_4\,C_2}{4\left(C_o + C_1 - \frac{C_2}{2}\right)} \tag{69}$$

where the C coefficients are obtained from Eqs. (53). The value of ϵ given by Eq. (69) is adequate only for the case of small angle of attack and camber and depth chord ratios larger than about 1. For large angles of attack, large camber, and finite aspect ratio, it is pointed out in Ref. 3 that an effective depth of submersion $(d/c)_e$ should be used in determining the C coefficients in Eq. (69). The value of $(d/c)_e$ is the value of d/c on the $\alpha = 0$ line in Fig. 2 corresponding to the value of $m = m_e$ where

$$m_e = \frac{C_L}{C_{L,\infty}}\,\frac{\pi}{2} = \frac{m\{\alpha + \alpha_c - \alpha_i\}}{m\{\alpha + \alpha_c - \alpha_i\}_\infty}\,\frac{\pi}{2}\,. \tag{70}$$

The value of the C coefficients are then determined for $(d/c)_e$ and $A_o = \alpha - \alpha_i$. It has been found after several calculations that the value of ϵ is not greatly affected by the depth of submersion.

Center of pressure—The linearized expression for the center of pressure of a finite-aspect-ratio, supercavitating hydrofoil operating at zero cavitation number and finite depth of submersion is

$$x_{c.p.,1} = \frac{C_{m,1}}{C_{L,1}} = \frac{1}{16}\;\frac{5C_0 + 7C_1 - 7C_2 + 3C_3 - \frac{C_4}{2}}{\left(C_0 + C_1 - \frac{C_2}{2}\right)} \tag{71}$$

where the C coefficients are determined at the effective depth of submersion given by Eq. (70) and for $A_0 = \alpha - \alpha_i$. Superimposed on this flow is the crossflow component of lift which is assumed to be distributed uniformly over the chord and acting in a direction normal to the chord line. Thus, the distance from the leading edge to the center of pressure of the crossflow-lift component $x_{c.p.,c}$ is given by

$$x_{c.p.,c} = 0.5c\,. \tag{72}$$

Admittedly, this assumption is crude and accurate only for a flat plate. For cambered surfaces the crossflow will not be uniformly distributed and for low-drag cambered sections such as the five-term section the crossflow is probably concentrated on the rearward portion of the hydrofoil.

By combining Eqs. (71) and (72) the center of pressure of the combined flows is, therefore,

$$x_{c.p.} = \left(\frac{C_{L,1}\,x_{c.p.,1} + 0.5C_{L,c}}{C_L}\right)c\,. \tag{73}$$

As in the case of ϵ, a few calculations reveal that a fair approximation for $x_{c.p.,1}$ is obtained by using $C_0 = \alpha - \alpha_i$ and $C_n = A_n$ in Eq. (71).

Comparison Between Theory and Experiment

Lift—In Fig. 12 the lift coefficient as given by Eq. (67) is compared with experimental data obtained on four different hydrofoils operating ventilated near the free surface. These models were

1. Flat plate, aspect-ratio-1, $d/c = 0.071$
2. Tulin-Burkart section, $C_{L,d} = 0.392$, aspect-ratio-1, $d/c = 0.071$
3. Five-term section, $C_{L,d} = 0.392$, aspect-ratio-1, $d/c = 0.141$
4. Five-term section, $C_{L,d} = 0.196$, aspect-ratio-3, $d/c = 0.141$.

The models were tested in Langley tank No. 2 at speeds between 20 and 80 fps and in the high-speed facility at speeds up to 180 fps. All force and moment coefficients obtained in the ventilated condition were found to be independent of speed. It may be seen that the experimental lift coefficients obtained were in excellent agreement with the theory.

In Fig. 13 the theory is compared with experimental data obtained on the four models at an angle of attack of 20 degrees operating ventilated for a range of depths of submersion. Again the theory is in excellent agreement with the data. It should be noted that the depth of submersion over the range of d/c from 0 to 1.0 has only a small effect on the value of C_L, particularly for the highly cambered model 3. The greatest influence of depth is found for the flat plate where the lift coefficient at zero depth is about 25% greater than that claculated for the infinite depth.

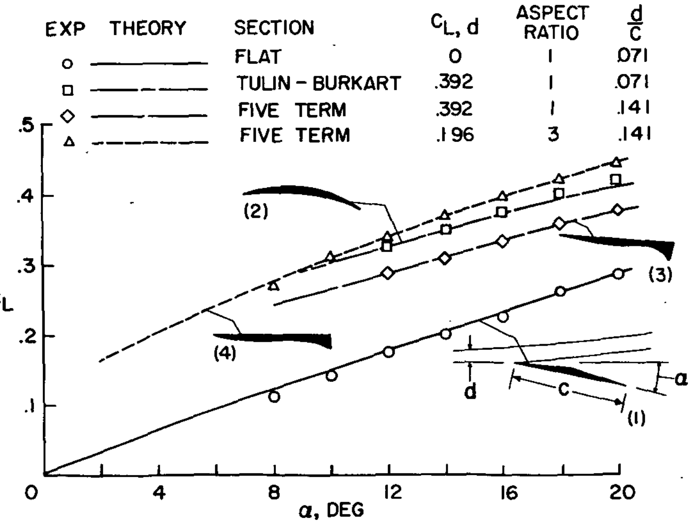

Fig. 12 - Lift coefficients of four low-aspect-ratio hydrofoils

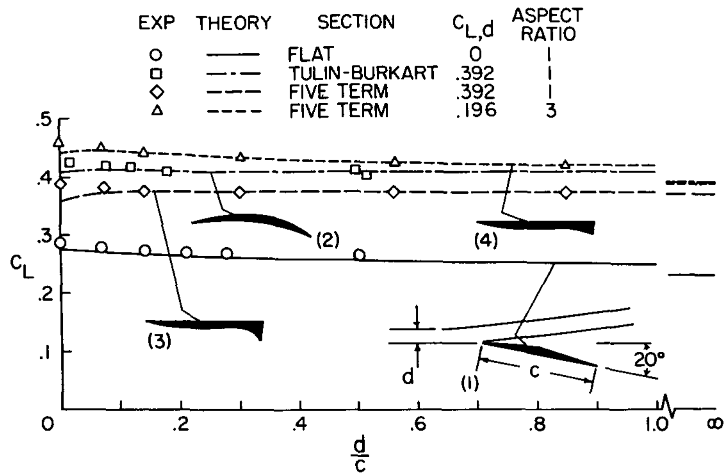

Fig. 13 - The influence of depth of submersion on the lift coefficient of four low-aspect-ratio hydrofoils (α = 20 degrees)

Drag—In Fig. 14 the drag coefficients of the four models obtained from experiment are compared with the theoretical values computed from equation (68). The agreement is excellent except for the highly curved model 3. The deviation between theory and experiment for model 3 is attributed to the inability of the linearized theory to accurately predict the pressure distribution when the camber is so gross. On a shape such as the five-term section only a small error in pressure distribution can greatly influence the drag without appreciably affecting the lift.

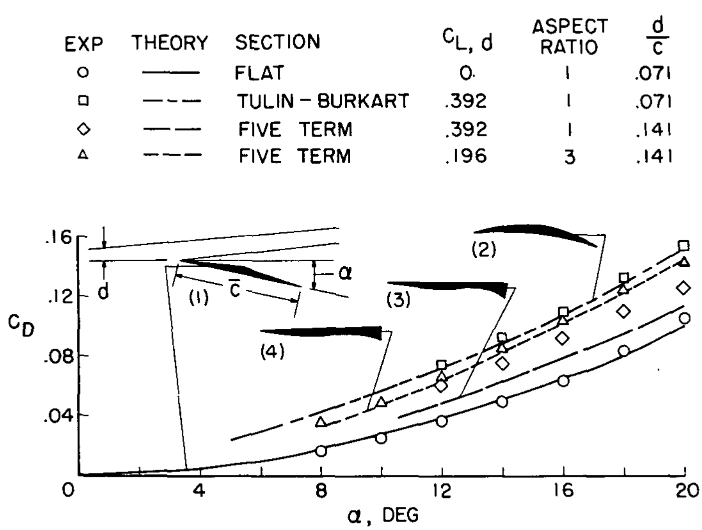

Fig. 14 - Drag coefficient of four low-aspect-ratio hydrofoils (excluding friction)

Center of Pressure—In Fig. 15 a comparison is made between the centers of pressure determined from Eq. (73) and those obtained experimentally on the four models. The theory is in good agreement with the data obtained on models 1 and 2, and about 10% too low on models 3 and 4.

LOCATION OF UPPER CAVITY STREAMLINE

The desirability of operating as near the design lift coefficient as possible is obvious from Fig. 4. Therefore, the minimum angle at which a hydrofoil with a finite thickness can operate with a cavity from the leading edge is needed. The angle can be determined by determining the location of the upper cavity streamline. The minimum angle at which this upper cavity streamline clears the upper surface of a hydrofoil of finite thickness is the angle desired. An approximate solution for the location of the cavity streamline is derived in the following analysis.

Two-Dimensional Theory-Arbitrary Depth

Green's Exact Solution for Flat Plate—The equation of the upper cavity streamline for a two-dimensional flat plate may be obtained from the solution of Green as

$$x/\delta = \frac{1}{\pi(b - \cos\alpha)}\left[\cos\alpha(t-1) - (1 - b\cos\alpha)\ln\frac{t-b}{b-1}\right] \tag{74}$$

$$\ell/\delta = \frac{\sin\alpha}{(b-\cos\alpha)}\left[\sqrt{t^2-1} + b\ln\left(t+\sqrt{t^2-1}\right) - \sqrt{b^2-1}\ln\left(\frac{b\,t-1+\sqrt{b^2-1}\sqrt{t^2-1}}{t-b}\right)\right] \tag{75}$$

where x is distance from the leading edge along the plate, ℓ is the perpendicular distance from the lower surface of the plate to the cavity streamline, and δ is the spray

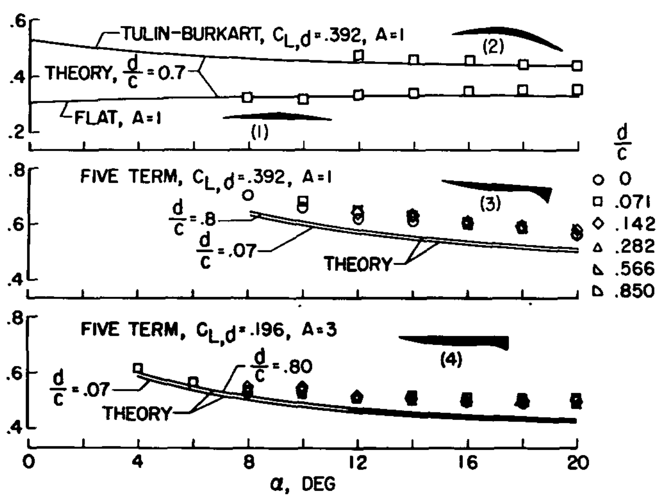

Fig. 15 - Location of center of pressure for four low-aspect-ratio hydrofoils

thickness. For a selected value of δ/c, b is known from Eq. (2b). Thus ℓ/c for a given x/c may be obtained by using the equations

$$\frac{x}{c} = \frac{x}{\delta}\ \frac{\delta}{c}, \qquad \frac{\ell}{c} = \frac{\ell}{\delta}\ \frac{\delta}{c} \tag{76}$$

and Eq. (75) for various values of the parameter t. The cavity streamline computed in this manner for several angles of attack and spray-thickness-to-chord ratios are presented in Fig. 16. The subscript A_o on $(\ell/c)_{A_o}$ is to indicate cavity ordinate due to angle of attack. It can be seen in Fig. 16 that for finite depths the cavity streamline rapidly approaches a straight line. The angle between this line and the plate is denoted as $\varphi + \alpha$ and is given in Ref. 4 as

$$\varphi + \alpha = \frac{b \cos \alpha - 1}{b - \cos \alpha}\ . \tag{77}$$

The magnitude of $\varphi + \alpha$ is shown for each streamline in Fig. 16. In Fig. 10 it may be seen that the cavity ordinate varies almost linearly with angle of attack for angles less than about 8 degrees. The value of $(\ell/c)_{A_o}/\alpha$ or more generally $(\ell/c)_{A_o}/A_o$ can be readily obtained and is given in Fig. 17. The value of $(\ell/c)_{A_o}/A_o$ for infinite depth is the same as the linearized result obtained in Ref. 1. Figure 17 shows that the cavity ordinates at a depth of about 0.5 chord are nearly twice as great as those obtained at infinite depth.

The Linearized Solution for Cambered Sections—In order to determine the cavity ordinates for a cambered section it is necessary to use the rigorous linearized solution previously discussed in the section on forces and moments. The problem of obtaining the hydrofoil cavity ordinates is simple in principle. All that is required is to find the vertical velocity perturbations $\bar{v}(-\bar{x}/\bar{c})$ ahead of the equivalent airfoil shown in Fig. 6. The value of $\bar{v}$ is needed because from it the value of v on the hydrofoil cavity streamline can be found. Since the linearized slope of the cavity streamline dy/dx is v/V, the shape of the cavity is determined.

The procedure for determining the vorticity distribution Ω on the airfoil is exactly the same as the first three steps given in the procedure for determining the linearized solution for the forces and moments. The value of $\bar{v}(\bar{x}/\bar{c})$ can be determined by integrating the increments of $\bar{v}$ induced at a point $-\bar{x}/\bar{c}$ due to the distributed vorticity Ω given by Eqs. (10) and (11). Obviously this integration becomes very complicated, particularly if there are many terms in $\Sigma A_n \sin n\theta$. The problem can be simplified however by dividing the velocity $\bar{v}$ into two parts, $\bar{v}_{A_o}$ and $\bar{v}_c$, where $\bar{v}_{A_o}$ is the component contributed by the first term $A_o \cot \theta/2$, and $\bar{v}_c$ the component contributed by the camber terms, $\Sigma A_n \sin n\theta$. Thus the final nondimensional cavity ordinates ℓ/c will be broken down into two components $(\ell/c)_{A_o}$ and $(\ell/c)_c$ such that

$$(\ell/c)_{total} = (\ell/c)_{A_o} + (\ell/c)_c\ . \tag{78}$$

The distance ℓ is measured from the reference line of the section along a line normal to the reference line. There are two advantages to dividing the vorticity into its angle of attack and camber components. First, the value of $(\ell/c)_{A_o}$ is known from Green's solution and has been given in Fig. 16. The linearized version is shown in Fig. 17. Thus, half the job is done if A_o is known or can be determined.

It is now important to review the meaning of the coefficient A_o. The angle of attack is measured from the orientation which makes $A_o = 0$ when the depth is infinite. At this orientation and infinite depth

$$A_o' = -\frac{1}{\pi}\int_0^{\pi} \frac{d\bar{y}}{d\bar{x}}\, d\theta = 0 \tag{79}$$

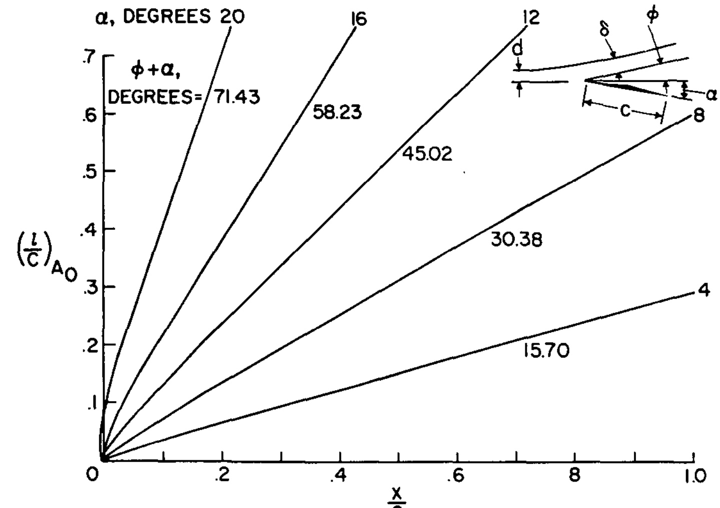

(a)

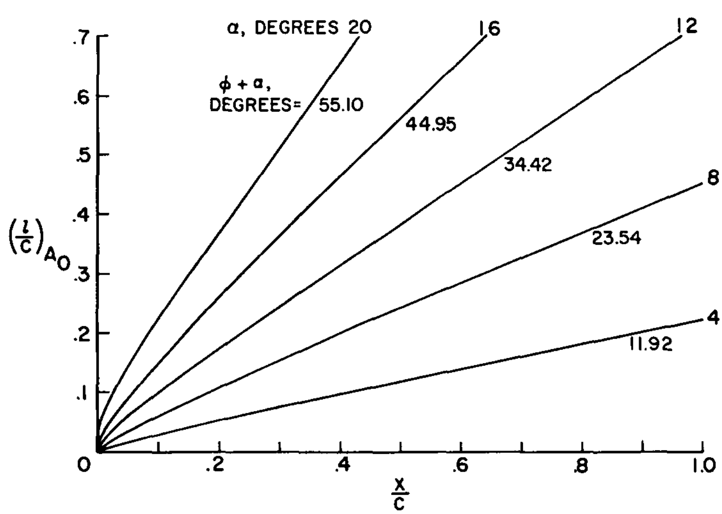

(b)

Fig. 16 - Green's solution for the upper cavity streamline of a flat plate. (a) $\delta/c = 0.25$, (b) $\delta/c = 0.50$, (c) $\delta/c = 1.0$, (d) $\delta/c = 2.0$, (e) $\delta/c = 5.0$.

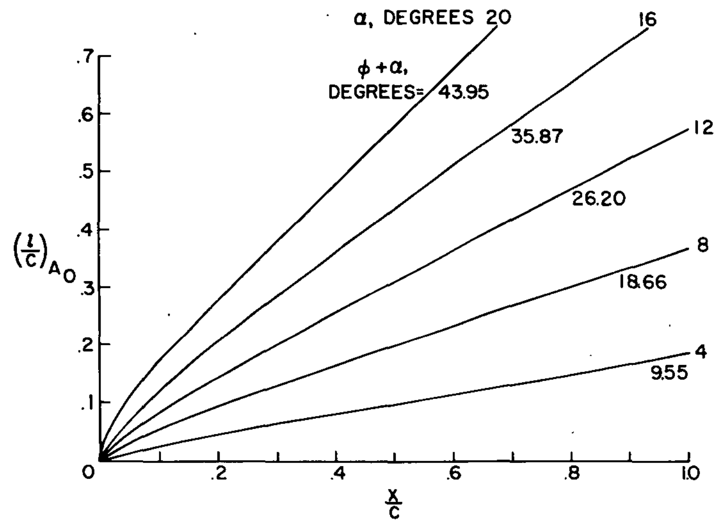

(c)

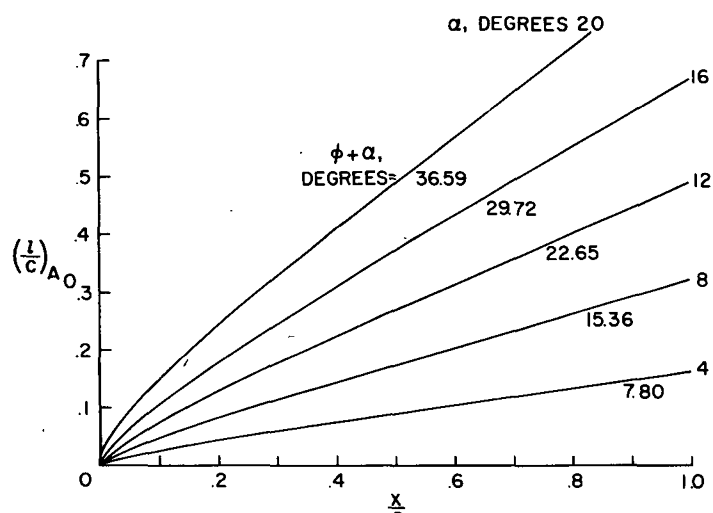

(d)

Fig. 16 (Continued) - Green's solution for the upper cavity streamline of a flat plate. (a) $\delta/c = 0.25$, (b) $\delta/c = 0.50$, (c) $\delta/c = 1.0$, (d) $\delta/c = 2.0$, (e) $\delta/c = 5.0$.

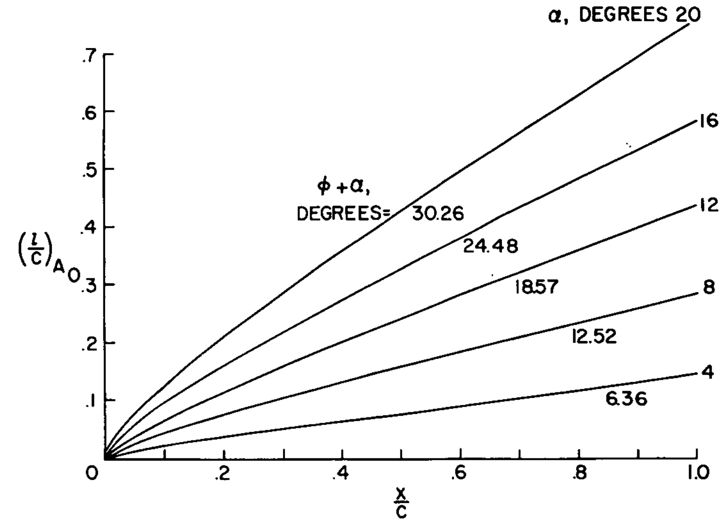

(e)

Fig. 16 (Continued) - Green's solution for the upper cavity streamline of a flat plate. (a) $\delta/c = 0.25$, (b) $\delta/c = 0.50$, (c) $\delta/c = 1.0$, (d) $\delta/c = 2.0$, (e) $\delta/c = 5.0$.

and for angles of attack measured from this reference orientation, $A_o = \alpha$. However if the angle of attack is measured from this reference line at finite depths it is found that the value of $A_o' \neq 0$. This means that at finite depths there is an induced angle of attack A_o' due to the camber. The magnitude of A_o' is directly proportional to the slope of the foil and thus to $C_{L,d}$. The calculated value of $A_o'/C_{L,d}$ is given in Fig. 18 for the four sections of interest for a range of depth-chord ratios. To obtain the value of $(\ell/c)_{A_o}$, one obtains A_o' from Fig. 18 and A_o by adding α; that is, $A_o = \alpha + A_o'$. Then $(\ell/c)_{A_o}$ is obtained from Fig. 16 or 17.

The second reason for dividing the vorticity distribution into the A_o and camber contributions is that the $\Sigma A_n \sin n\theta$ contribution usually has only small strength near the leading edge. In fact for low-drag sections, it is desirable to distribute the vorticity as near the trailing edge as possible. Thus the velocity induced at points ahead of the airfoil due to the $\Sigma A_n \sin n\theta$ or camber contribution may be adequately approximated by concentrating the entire camber vorticity at one point, the center of pressure a, as shown in Fig. 19. The value of a is given by $\bar{C}_m/\bar{C}_L$ or

$$a = \frac{\left(A_o + A_1 - \frac{A_2}{2}\right)}{A_o + \frac{A_1}{2}} . \tag{80}$$

The strength of the singular vortex can be obtained from the equations

$$L_c = \rho \Gamma_c V = C_L \bar{c} \frac{\rho}{2} V^2 = \pi A_1 \bar{c} \frac{\rho}{2} V^2 .$$

Therefore

$$\Gamma_c = \pi \bar{c} V \frac{A_1}{2} . \tag{81}$$

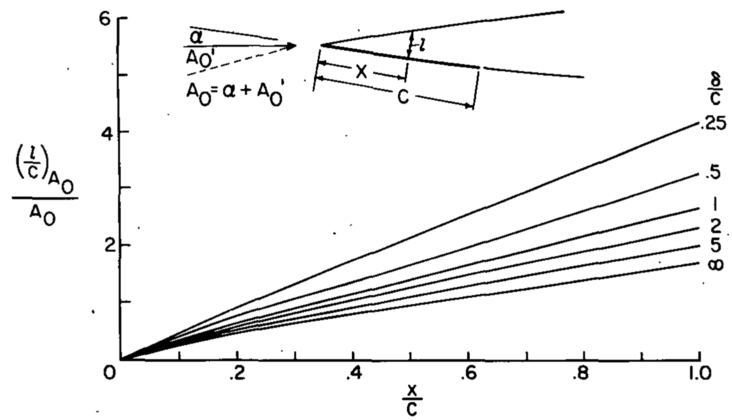

Fig. 17 - The linearized solution for cavity ordinates due to angle of attack

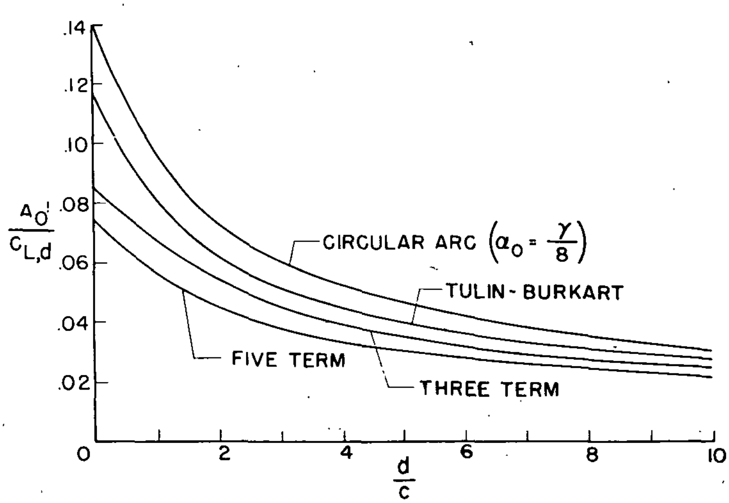

Fig. 18 - The influence of depth of submersion on the angle of attack induced by camber

The velocity induced at a point on the $\bar{x}$ axis due to Γ_c is therefore

$$\bar{v} = \frac{\Gamma_c}{2\pi(a\bar{c} - \bar{x})} = \frac{\pi \bar{c} V \frac{A_1}{2}}{2\pi\left(a\bar{c} - \frac{x}{c}\,\bar{c}\right)} = \frac{V \frac{A_1}{2}}{2\left(a - \frac{\bar{x}}{\bar{c}}\right)} . \tag{82}$$

The velocity $\bar{v}$ in front of the airfoil at a point $-\bar{x}/\bar{c}$ is exactly the same as v on the cavity streamline if the relationship between $-\bar{x}/\bar{c}$ and x/c given in Fig. 7 is maintained. Thus v/V and therefore the slope of the cavity streamline due to camber $dy/dx\ (x/c)$ is known. Integrating dy/dx from the leading edge to a point x/c gives

$$\left(\frac{\ell}{c}\right)_c = \int_0^{x/c} \frac{dy}{dx}\left(\frac{x}{c}\right) d\,\frac{x}{c} . \tag{83}$$

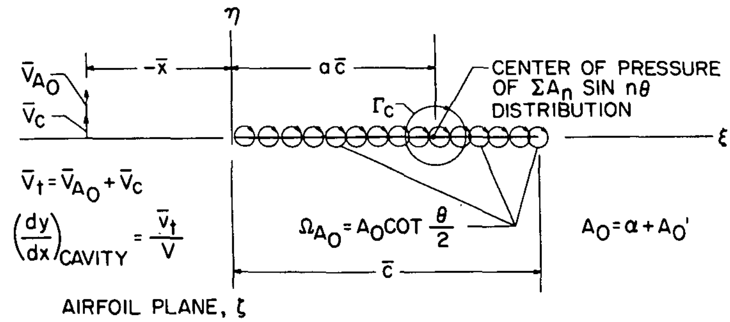

Fig. 19 - Linearized model for calculating upper cavity streamline at arbitrary depth

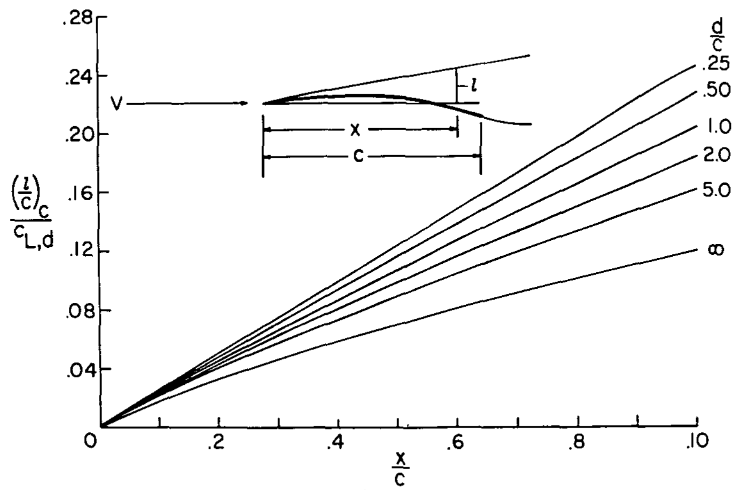

(a)

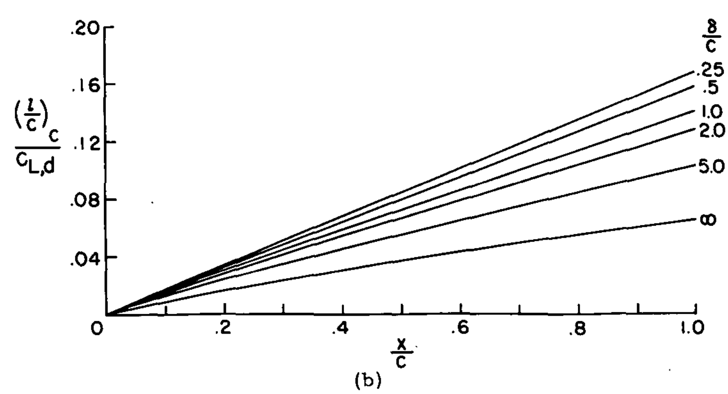

(b)

Fig. 20 - The influence of depth of submersion on the cavity ordinates due to camber: (a) circular-arc hydrofoil ($a_0 = \gamma/8$), (b) Tulin-Burkart hydrofoil

Therefore, since $dy/dx\,(x/c) = v/V$, and $v = \bar{v}$, combining Eqs. (82) and (83) gives

$$\left(\frac{\ell}{c}\right)_c = \frac{A_1}{4}\int_0^{x/c} \frac{d\frac{x}{c}}{\left(a - \frac{\bar{x}}{\bar{c}}\right)} \qquad (84)$$

where $\bar{x}/\bar{c}$ takes on negative values and the relationship between $-\bar{x}/\bar{c}$ and x/c is found in Fig. 7. Since $C_{L,d}$ is a function of A_1, then $(\ell/c)_c/C_{L,d}$ can be determined from Eq. (83). The magnitude of $(\ell/c)_c/C_{L,d}$ as a function of the depth/chord ratio is presented in Fig. 20 for the four sections of interest. Thus the total ordinates of the upper cavity streamline are obtained for the two-dimensional hydrofoil operating at zero cavitation number and arbitrary depth by using Figs. 16, 18, and 20 and Eq. (78).

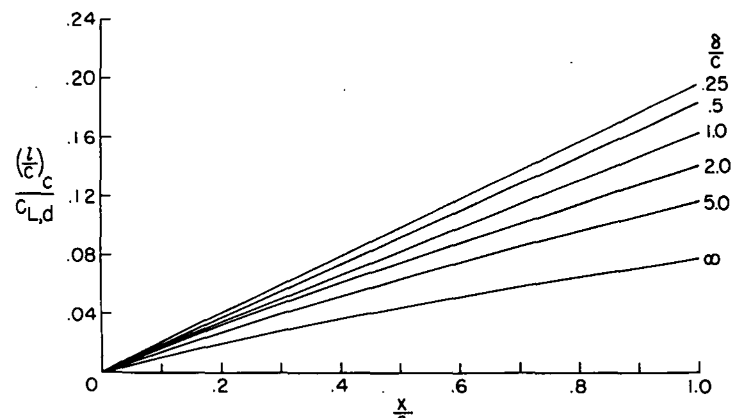

(c)

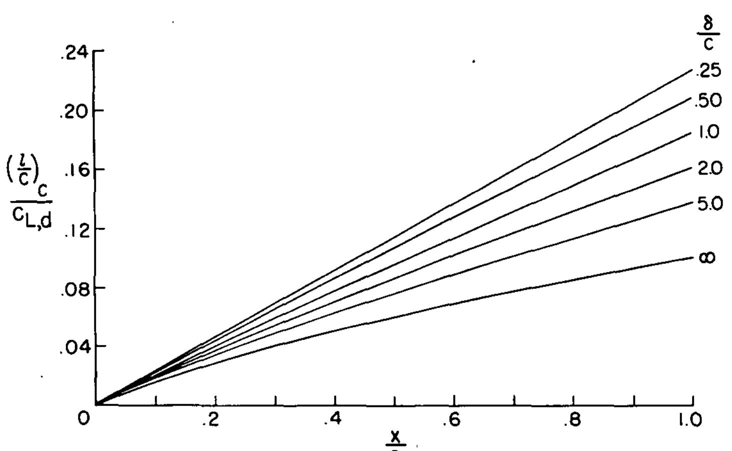

(d)

Fig. 20 (Continued) - The influence of depth of submersion on the cavity ordinates due to camber: (c) three-term hydrofoil, (d) five-term hydrofoil

Correction for Finite Aspect Ratio

Equation (82) shows that the cavity ordinates are directly proportional to the circulation on the equivalent airfoil and thus the circulation of the hydrofoil. Therefore, if the hydrofoil circulation is reduced from its two-dimensional value by finite span, the cavity ordinates must also reduce. Another argument for this decrease in cavity ordinates is that if the two-dimensional drag coefficient is reduced because of finite aspect ratio the maximum cavity thickness must also decrease as pointed out in Ref. 17. It is now assumed that for finite aspect ratios the cavity ordinates will be reduced from the two-dimensional value in proportion to the reduction in $C_{L,1}$. This reduction occurs in two places, first because of the reduced angle α_i and because of the reduced lift-curve slope m. More specifically, assuming the cosine terms are about equal to unity, the first term of Eq. (67) can be written as

$$C_{L,1} = \frac{A}{A+1} m_{(\alpha+\alpha_c-\alpha_i)}(\alpha - \alpha_i) + \frac{A}{A+1} m_{(\alpha+\alpha_c-\alpha_i)}\alpha_c \tag{85}$$

where the subscripts on m indicate the angle at which m is determined on Fig. 2. If α_c is broken into two components A_o' and α_c', that is, $\alpha_c = A_o' + \alpha_c'$, Eq. (85) becomes

$$C_{L,1} = \frac{A}{A+1} m_{(\alpha+\alpha_c-\alpha_i)} (\alpha + A_o' - \alpha_i) + \frac{A}{A+1} m_{(\alpha+\alpha_c-\alpha_i)} \alpha_c'. \tag{86}$$

The value of the cavity ordinates at infinite aspect ratio and angle $\alpha + A_o' - \alpha_i$ is

$$(\ell/c)_{total} = (\ell/c)_{(A_o-\alpha_i)} + (\ell/c)_c \tag{87}$$

where $(\ell/c)_{(A_o-\alpha_i)}$ is determined from the nonlinear solution of Green and $(\ell/c)_c$ from the linearized theory. Therefore the effective lift-curve slope at infinite aspect ratio and angle $A_o - \alpha_i$ is $m_{(A_o-\alpha_i)}$ for the first term in Eq. (87) and $m_{(\alpha=0)}$ for the second term. Thus at finite aspect ratio the corrected cavity ordinates are

$$(\ell/c)_{total} = \frac{\frac{A}{A+1} m_{(\alpha+\alpha_c-\alpha_i)}}{m_{(A_o-\alpha_i)}} (\ell/c)_{(A_o-\alpha_i)} + \frac{\frac{A}{A+1} m_{(\alpha+\alpha_c-\alpha_i)}}{m_{(\alpha=0)}} (\ell/c)_c \tag{88}$$

or

$$(\ell/c)_{total} = R_{A_o}(\ell/c)_{(A_o-\alpha_i)} + R_c(\ell/c)_c \tag{89}$$

where

$$R_{A_o} = \frac{A}{A+1} \frac{m_{(\alpha+\alpha_c-\alpha_i)}}{m_{(A_o-\alpha_i)}}$$

$$R_c = \frac{A}{A+1} \frac{m_{(\alpha+\alpha_c-\alpha_i)}}{m_{(\alpha=0)}} .$$

The preceding analysis assumes that the induced angle α_i is constant over the span. Since α_i actually varies over the span, except for the case of elliptic loading, the cavity ordinates will also vary over the span. This effect can be included by using the appropriate spanwise distribution of α_i determined from finite span airfoil theory (14). Also the influence of the crossflow component of flow on the cavity ordinates has been assumed to be negligible. However, near the tips the cavity shape is largely determined by the crossflow. For example, at zero aspect ratio the cavity is entirely determined by crossflow. Thus, it seems that the true cavity shape is determined at the tips by the crossflow and at the center by the main flow; the cavity shape in between is some transition between the two extremes.

Comparison Between Theory and Experiment

Figure 21a shows an aspect ratio one flat plate operating at a depth of 0.05 chord and an angle of attack of 16 degrees. The plate had 3 pins located along the span so that the upper ends of the pins were 0.34 chords rearward of the leading edge and 0.17 chords from the lower surface of the plate. These pins were spaced 0.021, 0.198, and 0.375 chords from the right tip of the plate. From the photograph the cross section of the cavity may be estimated as shown by the solid line in Fig. 21b. The horizontal dashed line is the calculated location based on a uniform distribution of α_i. The other dashed curve is the calculated streamline assuming the airfoil induced angle distribution for a rectangular plan form (14). It may be noted that near the tips the cavity shape is primarily due to crossflow, whereas near the center the calculated value based on the more nearly exact distribution of induced angle of attack is nearly correct if the draw-down due to the strut is overlooked. The cavity shape based on uniform induced angle distribution is about 20 percent too low.

In Fig. 22 the calculated cavity shapes based on uniform α_i are presented for two aspect-ratio-one hydrofoils operating at $d/c = 0.5$. It may be seen in Fig. 22a that for the flat plate the calculated streamline at an angle of attack of 4 degrees just touches the upper surface of the model. If it is assumed that the speed is sufficiently high so that no significant negative pressure coefficient can exist in the flow field, and if the forward portion of the upper surface is wetted and positive pressures occur, then the lift will decrease. Thus it may be concluded from the calculations that the maximum value of the lift/drag ratio for this flat plate hydrofoil should occur at the 4-degree angle of attack. Experimental data obtained at speeds up to 180 fps reveal that the forward portion of this flat-plate hydrofoil does become wetted at an angle of attack of about 4 degrees. The maximum lift/drag ratio also occurred at an angle of attack of about 4 degrees.

The hydrofoil section shown in Fig. 22b has a lower surface conforming to the Tulin-Burkart profile with $C_{L,d} = 0.392$. The details of the upper surface may be found in Ref. 3. The calculated location of the cavity streamline is shown for angles of attack of 4, 8, and 12 degrees. It may be noted that the calculated streamlines are almost identical with those shown in Fig. 22a for the flat plate. The reason that both foils have about the same theoretical cavity streamline location is peculiar to the

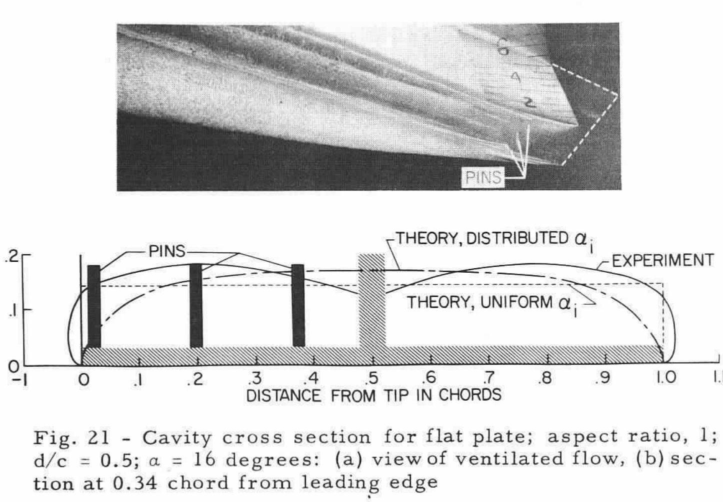

Fig. 21 - Cavity cross section for flat plate; aspect ratio, 1; $d/c = 0.5$; $\alpha = 16$ degrees: (a) view of ventilated flow, (b) section at 0.34 chord from leading edge

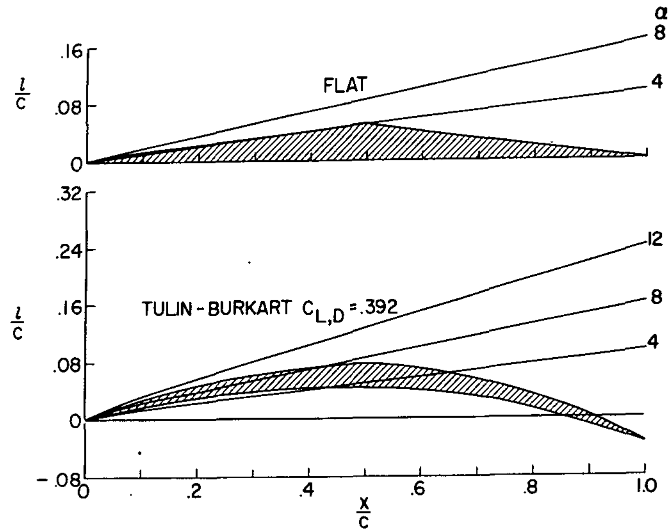

Fig. 22 - Calculated cavity shapes for flat and cambered models; aspect ratio, 1; d/c = 0.5

aspect ratio of 1. There are two compensating effects due to camber which cause this similarity in streamlines. The cambered foil cavity ordinates are increased because of the foil curvature, but simultaneously the camber causes increased lift at a given angle which produces a greater induced angle of attack. The greater induced angle of attack results in a decrease in cavity ordinates, thus effectively cancelling out the increased ordinates contributed by the foil curvature. Experimental data on both foils were in agreement with this theoretical phenomenon; in fact, at a 20-degree angle of attack the flat-plate cavity streamline obtained from both theory and experiment was slightly higher than that obtained for the cambered model.

Figure 22b indicates that ventilation from the leading edge of the cambered model will not be possible at angles less than about 10 degrees. Experiments conducted in ventilated flow up to speeds of 180 fps were in excellent agreement with this prediction; that is, at angles less than 10 degrees the forward portion of the upper surface was wetted. However, the maximum lift/drag ratio of the cambered model occurred at an angle of attack of about 7 to 8 degrees. The fact that the lift/drag ratio continued to increase even with the upper surface wetted is attributed to the curvature of the upper surface and finite speed. At a speed of 175 fps it is possible to support a negative pressure coefficient as low as -0.07. Thus, it is possible at finite speeds for the upper surface to add to the lift and possibly decrease the drag. Theoretically at higher speeds the maximum lift/drag ratio will occur closer to the predicted 10-degree angle of attack.

THEORETICAL COMPARISON OF PRACTICAL LOW-DRAG SECTIONS

The experimental data given in the preceding section indicate that a reliable approximation to the cavity streamline location on high-speed moderate-aspect-ratio surfaces can be obtained theoretically. Using the theory developed, it is now possible to determine the best of the four section shapes (circular-arc, Tulin-Burkart, three-term, and five-term) when operating under practical conditions. The operating condition chosen for comparison was at a depth of submersion of 1 chord and an aspect ratio of 3. The structural characteristics of the section were arbitrarily chosen as (a) thickness ratio $t/c = 0.03$ at 0.2 chord from the leading edge and (b) $t/c = 0.04$ at the chordwise location of the maximum lower surface ordinate. The leading edge and these control points were assumed to be connected by straight lines and the upper surface rearward of the latter control point was taken as parallel to the reference line of the section. Because of the almost uniform gradation of the various characteristics of the four sections, only the extremes, the circular-arc and five-term section, were compared.

Over the range of cambers from $C_{L,d} = 0$ to 0.3, the calculated cavity streamlines first touched the upper surface of the assumed hydrofoil sections at the 0.2-chord control point. Thus the second point at the maximum lower surface ordinate did not influence the maximum lift/drag ratio of the sections. The friction drag coefficient was estimated to be 0.004. Using Eqs. (67) and (68), the lift and drag coefficients of the sections were calculated. A plot of lift/drag ratio versus lift coefficient is presented in Fig. 23. Also shown in Fig. 23 is the line denoting the minimum angle at which the control point at 0.2 chord just clears the calculated cavity streamline. The area above this line is shaded to indicate that these regions are not attainable under the design conditions. The important result shown by these plots is that either type of camber can give higher maximum lift/drag ratios than the flat plate. The optimum amount of camber for both hydrofoils correspond to a value of $C_{L,d}$ of about 0.1. The optimum lift coefficient is about 0.175 for both sections. The hydrofoil cross sections shown in the top of Fig. 23 are for $C_{L,d} = 0.1$ oriented at the minimum angle of attack revealed by the analysis. The analysis as presented in Fig. 23 also shows that the five-term section is superior to the circular arc. The maximum values of the lift/drag ratios are 10.5 and 9.5 for the five-term and circular-arc sections respectively. Although L/D of the five-term section is slightly higher than that of the circular arc, it is not twice as high as predicted from the two-dimensional theory.

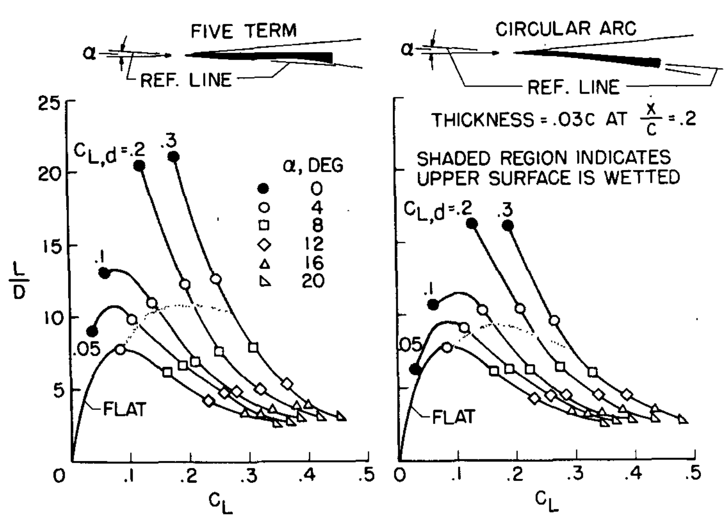

Fig. 23 - Theoretical lift/drag ratios of five-term and circular-arc hydrofoils; aspect ratio, 3; d/c = 1.0

The thickness distribution chosen for the analysis is not conservative, but a bare minimum. Structurally, an aspect ratio of 3 is close to the maximum when the hydrofoil is supported by a single strut. Therefore, the calculated maximum lift/drag ratio of about 10 at a lift coefficient of 0.18 is very near the optimum that can be obtained on a single supercavitating hydrofoil supported on one strut and operating at zero cavitation number. More severe structural requirements than those imposed in the present analysis will reduce the maximum attainable lift/drag ratio.

CONCLUDING REMARKS

In conclusion, it may be stated that the concept of combining the linearized effects of camber with nonlinear flat-plate theory has proved satisfactory. The results of a comparison of this theory, corrected for aspect ratio, with experimental data obtained on four low-aspect-ratio sections may be summarized as follows.

1. The theoretical lift coefficient was in excellent agreement with experimental data.

2. The theoretical drag coefficient was in excellent agreement with experimental data on all models except the highly cambered five-term section whose $C_{L,d} = 0.392$. The disagreement is attributed to the inability of linearized theory to accurately predict the pressure distribution when the curvature is very great.

3. The theory predicts centers of pressures slightly low for the five-term section; however, the agreement may be improved by taking the center of pressure of the crossflow component rearward of the mid-chord.

4. Theoretical cavity shapes based on a uniform induced angle of attack are in good enough agreement with experiment to warrant their use in engineering calculations.

Using the theory presented and selecting sections of similar structural geometry, it is shown that the highest lift/drag ratio that can be obtained on a ventilated hydrofoil supported by a single strut at depths of 1 chord or more is about 10. The best section for optimum lift/drag ratio is the five-term design; however, the camber profile may range from the five-term to the circular arc with only about a 10 percent change in the maximum lift/drag ratio.

REFERENCES

1. Tulin, M.P., and Burkart, M.P., "Linearized Theory for Flows About Lifting Foils at Zero Cavitation Number," Rept. C-638, David W. Taylor Model Basin, Navy Dept., Feb. 1955

2. Johnson, V.E., Jr., "Theoretical Determination of Low-Drag Supercavitating Hydrofoils and Their Two-Dimensional Characteristics at Zero Cavitation Number," NACA RM L57G11a, 1957

3. Johnson, V.E., Jr., "Theoretical and Experimental Investigation of Arbitrary Aspect Ratio, Supercavitating Hydrofoils Operating Near the Free Water Surface," NACA RM L57I16, 1957

4. Green, A.E., "Note on the Gliding of a Plate on the Surface of a Stream," Proc. Cambridge Phil. Soc. XXXII(pt. 2):248-252 (May 1936)

5. Shuford, C.L., Jr., "A Theoretical and Experimental Study of Planing Surfaces Including Effects of Cross Section and Plan Form," NACA TN 3939, 1957

6. Perry, B., "Experiments on Struts Piercing the Water Surface," Rept. E-55.1 (Contract N123s-91875), C.I.T., Hydrod. Lab., Dec. 1954 (available from ASTIA as AD No. 56179)

7. Eisenberg, P., "On the Mechanism and Prevention of Cavitation," Rept. 712, David W. Taylor Model Basin, Navy Dept., July 1950

8. Wadlin, K.L., Ramsen, J.A., and Vaughan, V.L., Jr., "The Hydrodynamic Characteristics of Modified Rectangular Flat Plates Having Aspect Ratios of 1.00, 0.25, 0.125 and Operating Near a Free Water Surface," NACA Rep. 1246, 1955 (supersedes NACA TN's 3079 by Wadlin, Ramsen, and Vaughan and 3249 by Ramsen and Vaughan)

9. Lamb, H., "Hydrodynamics," reprint of sixth ed. (first American ed.) Dover Publications, 1945

10. Milne-Thompson, L.M., "Theoretical Hydrodynamics," 2nd ed., MacMillan and Co., Ltd., 1949

11. Rosenhead, L., "Resistance to a Barrier in the Shape of an Arc of Circle," Proc. Roy. Soc. (London) A117(No. 777):417-433 (Jan. 2, 1928)

12. Wu, T. Yao-tsu, "A Free Streamline Theory for Two-Dimensional Fully Cavitated Hydrofoils," Rept. 21-17 (Contract N6onr-24420), C.I.T., Hydrod. Lab., July 1955

13. Wagner, H., "Planing of Watercraft," NACA TM 1139, 1948

14. Glauert, H., "The Elements of Airfoil and Airscrew Theory," 2nd ed., Cambridge Univ. Press, 1947 (reprinted 1948)

15. Jones, R.T., "Correction of Lifting-Line Theory for the Effect of the Chord," NACA TN 817, 1941

16. Flax, A.H., and Lawrence, H.R., "The Aerodynamics of Low-Aspect Ratio Wings and Wing-Body Combinations," Rept. CAL-37, Cornell Aero. Lab., Inc., Sept. 1951

17. Tulin, M.P., "Supercavitating Flow Past Foils and Struts," Proceedings of a Symposium on Cavitation in Hydrodynamics, National Physical Laboratory, Sept. 14-17, 1955

* * * * *

DISCUSSION

D. Savitsky (Stevens Institute of Technology)

I would like to congratulate Mr. Johnson on accomplishing a most clever combination of established aerodynamic and hydrodynamic results to develop practical solutions for a most difficult hydrodynamic problem. As is typical for semi-empirical approaches, the approximations used can often times be questioned and more refined approximations suggested. However, the choice is usually the author's to make and if the calculated results agree with data then he's chosen correctly.

Working within the framework developed by Mr. Johnson, I would like to address myself to the subject of the two-dimensional cavity shape associated with the design lift coefficient at various depths of submersion. The design lift coefficient is, as usual, that existing for the "shock-free" entry condition. The study of the cavity shape is, by far, the most pressing one since the intersection of the cavity with the foil's upper surface is the strongest obstacle in the way to achieving the very high lift-drag ratios which are potentially possible with super-cavitating hydrofoils.

In Fig. 20 of Mr. Johnson's paper a plot is shown of the influence of depth of submersion on the cavity ordinates due to the circulation developed by a cambered foil when operating with shock-free or design lift coefficient at infinite draft. It is seen in Fig. D1 that for a fixed value of circulation the cavity opens up as the free water surface is approached. Now it can be shown from Johnson's work that the design angle (shock-free) of attack for a given cambered section decreases with decreasing submersion while the design lift coefficient remains essentially constant. Using this result then, Fig. D1 can be interpreted as representing the cavity shape relative to the horizon when a given circular-arc hydrofoil is maintained at a constant design lift coefficient by reducing the geometric chord line angle of attack when approaching the free-surface. Superposed on Fig. D1 is a circular arc hydrofoil

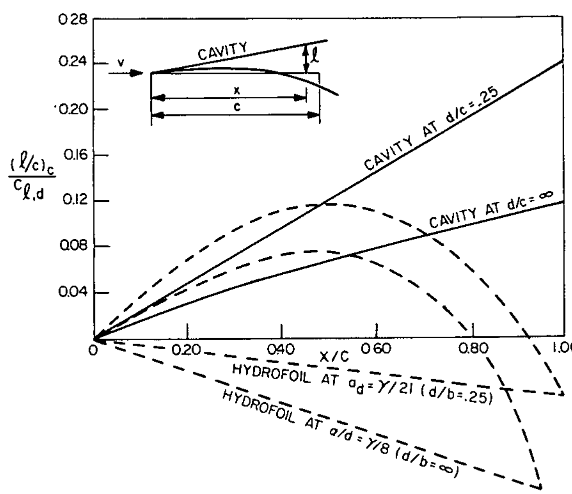

Fig. D1 - Cavity ordinates for circular-arc hydrofoil--Johnson's results oriented to the design angle of attack for $d/c = \infty$ and $d/c = .25$. It is seen that the intersection of the cavity with the hydrofoil is, within engineering accuracy, very nearly the same for the entire range of submersion.

Figure D2 shows the collapsed results and points up that the cavity interaction with the hydrofoil can be represented by one curve for all depths of submersion when the foil is maintained at design lift coefficient. In effect then, while the cavity does open up as the free-surface is approached, we rotate the foil into the cavity as the geometric angle of attack is decreased to maintain the design lift coefficient.

Hence, the problem of the cavity shape is equally obstructive at all drafts and whatever can be done to alleviate the cavity interference problem at one draft should probably hold at other drafts.

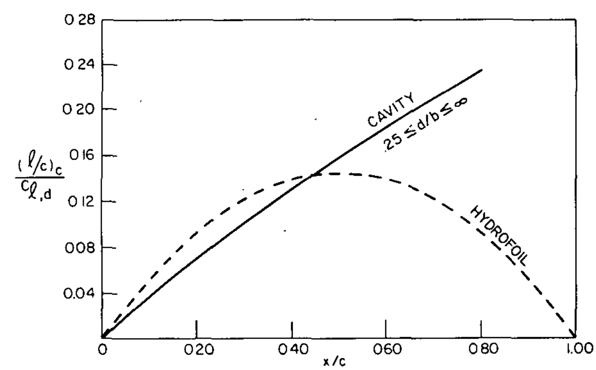

Fig. D2 - Cavity ordinates for circular-arc hydrofoil—collapsed results for hydrofoil at design angle of attack corresponding to each draft

M. C. Eames (Naval Research Establishment, Halifax)

I think I am correct in saying that Mr. Johnson's paper presents more information of use to the practical designer than can be found in any single paper on conventional hydrofoils. That this has been accomplished so rapidly in this new field of supercavitating hydrofoils is a remarkable achievement.

I would like to supplement Mr. Johnson's introduction from the point of view of the surface ship - as opposed to that of the aircraft.

It is well known that the limit on speed resulting from cavitation on conventional hydrofoils implies a corresponding size limit due to the so-called "square-cube" law. That is to say, as the size of craft is increased, retaining a constant design speed, the required size of the hydrofoils increases rapidly, and the weight associated with the hydrofoils soon becomes a prohibitive proportion of the total displacement.

Attempts at delaying cavitation to higher speeds are of limited value because they imply lower lift coefficients, and hence, again, large hydrofoils.

Thus to the surface ship designer, the successful development of supercavitating hydrofoils offers the possibility - at least - of radical increases in the size of vessel for which hydrofoil support is feasible. There will be serious engineering problems involved in the design of large hydrofoil ships, but there no longer appears to be any fundamental objection to increasing size.

Undoubtedly the most important contribution made by the NACA work is the concept of using a fully-ventilated cavity. Prior to this development, three regimes of design were recognized. Below a speed of about 40 knots, cavitation presented no problems provided reasonable lift coefficients were used, and it is fair to say that no problems remain in the design of hydrofoil craft up to this order of speed - accepting the size limitations that I have referred to. By careful foil selection it is possible to delay the onset of cavitation to about 60 knots, still retaining reasonable lift coefficients, but in this regime difficulties begin to be encountered in rough water. This is because the range of angle of attack over which cavitation free operation can be obtained is very limited. Moreover, with the type of section required here, the onset of cavitation is not a gradual process, but can be as sudden and abrupt as complete ventilation.

Above 60 knots it was thought that super-cavitation would take over. At this speed a fully developed vapour cavity would be feasible, but there remained the problem of ensuring that this would not ventilate.

Mr. Johnson's solution to this problem—refusing to solve it—is one of those delightfully simple touches that characterize a major technical break through. Not only does the "super-ventilating" foil, if I may use this term, solve the problem of stabilizing the cavity in the presence of a free surface, but it also means that the transition from conventional to super-cavitating operation can be made at a much lower speed. It is likely that the troublesome "cavitation delaying" hydrofoils required for operation in the 40-60 knot range have no place in future developments.

As many of you will be aware, the Naval Research Establishment in Halifax has been concerned with the development of hydrofoil craft in the 40-60 knot range of speeds, and this new concept is therefore of very great interest to us.

In the course of our work, in addition to the R-100 "Massawippi" and R-103 "Bras d'Or" hydrofoil craft, which have received a fair amount of publicity, we have developed a new research vehicle, known as the "R-X", which we intend to use for an investigation into the practical application of "super-ventilating" foils for surface craft.

The new R-X is not intended to represent a scale model of any possible operational prototype. It was designed as a basic research vehicle with the capability of exploring a wide range of hydrofoil configurations and types. A full description is out of place here, but it is felt that some of the unusual features which make this craft particularly suitable for fundamental studies will be of interest.

Figure D3 provides a general view of the 3-ton boat. The important feature of the 25-foot plywood hull is the aluminum rail (A) which runs the full length of each gunwale. By means of a slide attachment the main foil mounting structure (B) can be positioned at any point on the length of the hull. In Fig. D3, a three-point, two-leading, configuration is shown fitted. For a four-point, or tandem, configuration a second identical structure can be mounted aft.

Figure D4 shows a close-up of one of the main foil units. The mounting structure consists of a rigid athwartships beam (C), which is pivoted to the gunwale slides (D)

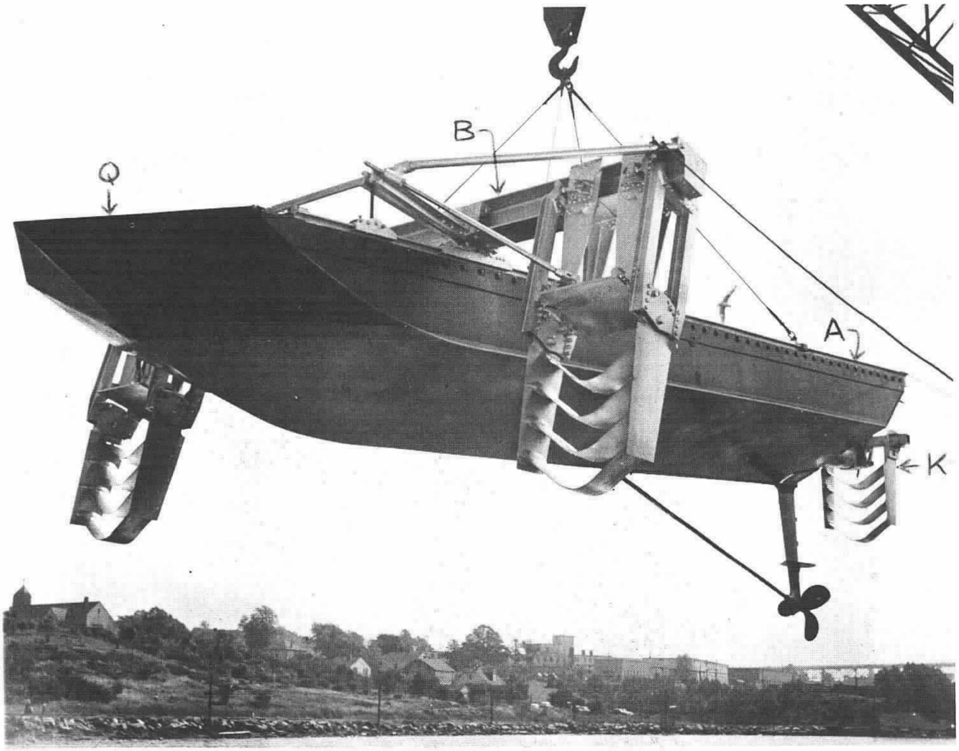

Fig. D3 - The R-X research craft

port and starboard. Change of rake or fine adjustment of incidence can be accomplished by means of a screw thread (E). Rigid cantilevers (F) can be clamped to the beam in any athwartships position thus providing for alteration of foil track, and of the span of individual foil units. The frames (G) which carry the foil struts are connected to the rigid cantilevers (F) only by way of dynamometer elements (H). There are four such elements to each strut, enabling lift, drag and cross force to be independently measured and recorded. This, and other instrumentation is currently being developed.

For three-point configurations, the stern unit (Fig. D3, K) is mounted on a telescopic tube fitted into the stern of the hull. By this means the fore and aft position of the stern unit can be varied over a distance of 5 feet. This is sufficient to investigate configurations in which the stern foil supports between 10 percent and 33 percent of the all-up weight without changing the foil base length. Figure D5 is a close-up of the stern unit, showing the telescopic tube (L), the steering bearings (M) and the mounting beam (N). The foil struts are attached by clamps (O), thus allowing for units of different span, while the beam (N) can be tilted for adjustment of rake or incidence by a screw thread device not visible in this view. The beam assembly is attached to the steering bearings only by way of four dynamometer elements (P).

For three point, one-leading, or "canard," configurations the telescopic tube can be removed from the stern of the craft, and fitted in the bow. This necessitates

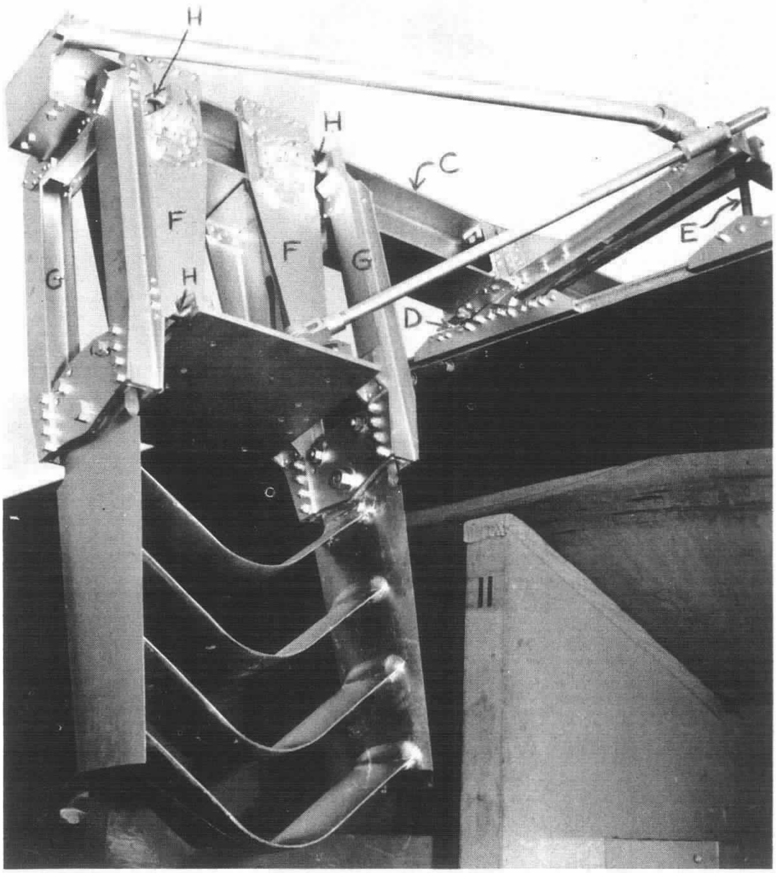

Fig. D4 - One of the main foil units

removal of the false bow (Fig. D3, Q), and steering would then be accomplished by turning the bow unit. The same mounting structure is used for the bow unit.

The craft is being powered by conventional means to provide a speed of at least 40 knots with a minimum lift-to-drag ratio of 5; instrumentation will include the recording of thrust, torque, r.p.m., pitch, roll, vertical accelerations and foil unit forces on a time base. A strut unit for measuring altitude, speed and angle of yaw is also being developed.

It is felt that the versatility of this craft is unique and that although "teething troubles" will no doubt be encountered, due to attempting to fit a quart into a pint pot, its potential value for extending laboratory experiments on ventilated hydrofoils to actual operating conditions is high.

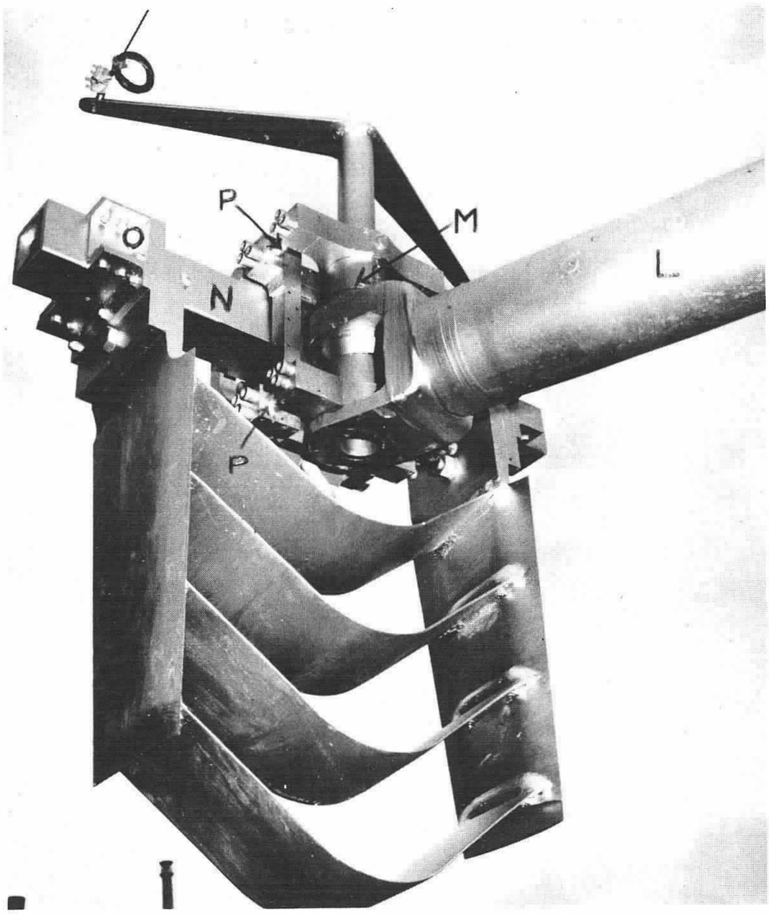

Fig. D5 - The stern foil unit

P. Ward Brown (Stevens Institute of Technology)

There is such a great wealth of information in Mr. Johnson's paper, and so many novel ideas scattered liberally throughout it, that it is perhaps ungracious to comment in any other way than by prolonged applause.

Nonetheless, I would like to discuss the method of calculating lift at finite depth. Mr. Johnson develops an ingenious, but approximate, linear solution for the lift of a supercavitated hydrofoil at finite depth. In order to improve the approximation he calculates the approximate lift at finite depth with a design angle of attack for infinite depth. Through this calculated point he draws a line having the slope given by Green's non-linear theory* at finite depth and design angle of attack for finite depth. It would seem to be more correct to calculate the lift at finite depth and at the design angle of attack for finite depth, and then to use the slope given by Green's theory.

*A.E. Green, "Note on the Gliding of a Plate on the Surface of a Stream," Proc. Camb. Phil. Soc., 32:248-252 (1936).

The difference between these two approaches for a circular-arc foil is shown in Figs. 1 and 2, for the case of zero depth. The lift curve for infinite depth is shown for reference.

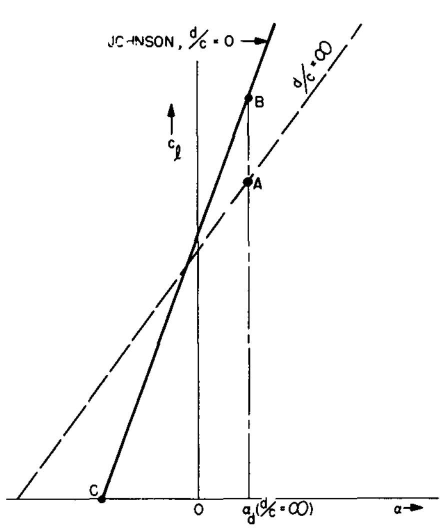

Fig. D6 - Effect of depth on lift coefficient – Johnson's method

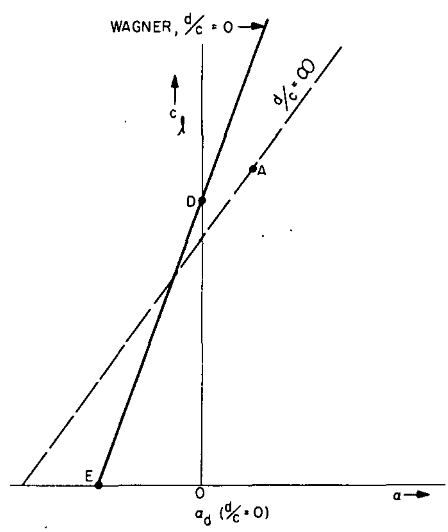

Fig. D7 - Effect of depth on lift coefficient – proposed method

Figure 1 shows Johnson's method. Point B is the lift calculated for zero depth at the design angle of attack for infinite depth and the line BC has the slope given by Green. The alternate method is shown in Fig. 2. Point D is calculated for zero draft and at the design angle of attack for zero draft. Again, DE has the slope given by Green but gives a different intercept on the lift axis.

It is interesting to note that the line DE given by the second method is exactly that predicted by Wagner† and the very small change in design lift coefficient with depth may also be noted. In fact according to Wu's non-linear theory‡ the design lift coefficient of a circular-arc hydrofoil at infinite depth is exactly the same as the design lift coefficient given by Wagner for zero depth.

It seems that the lift at finite depth might be written as follows;

$$C_\ell = m(d/c)\alpha/\alpha_d(d/c) + C_{\ell_d} \tag{1}$$

where the slope, m, and the design angle of attack, α_d, are both functions of the draft-chord ratio, (d/c), (as given by Green and Johnson, respectively) and the design lift coefficient, C_{ℓ_d}, is independent of draft.

†H. Wagner, "Planing of Watercraft," NACA TM 1139, 1948.

‡T.Y. Wu, "A Free Streamline Theory for Two-Dimensional Fully Cavitated Hydrofoils," C.I.T. Hydro Lab. Rep. No. 21-17, April 1955.

It is not always necessary to correct for depth effects. Recently at the Experimental Towing Tank, Stevens Institute of Technology, under contract with the Office of Naval Research, the lift and drag of a fully ventilated, surface-piercing, dihedral hydrofoil, has been measured. Analysis of the experimental results shows that after eliminating aspect ratio effects there is no residual depth effect. Thus a surface-piercing, dihedral foil has an effective draft-chord ratio of infinity. The tests also confirmed the linear slope, $\pi/2$, of the lift curve up to 16, but there was no fall off in lift as predicted by Wu's non-linear theory. However, the experimental design lift coefficient was only 70 percent of that predicted by the linear theory. The results of these tests will be published shortly.*

Hirsh Cohen and R. C. DiPrima

In reply to Marshall Tulin, we would like to say that we are in agreement with his remarks. What we were trying to point out was simply that the linearized theory that has been used to estimate boundary effects does give the correct qualitative effects, but does not, at least in the cases considered here (the 15° half angle wedge, and the flat plate at angle of attack of 12°), give the accuracy of a non-linear theory.

The question of slotted wall tunnels has been brought up by Dr. Silverleaf and by Prof. Silberman. It seems to us that judging from the results presented in this paper, little effect on force coefficients is to be expected. It seems reasonable to expect the results for force coefficients to lie between those for solid-wall and free-jet test sections. On the other hand, blockage effects on cavity dimensions are of some interest. For a given model and tunnel size, lower cavitation numbers may be obtained with a slotted wall tunnel. It certainly seems worthwhile to make blockage studies for the slotted wall case. There seems to be need of some caution in using such test sections, as proven by the instability problems experienced at A.R.L. The possibility of cavity-slotted wall instability interactions should be looked into.

Professor Silberman has raised a point which has, indeed, troubled us. He remarks that for very low cavitation numbers the drag on the 15° and 12.5° wedges is lower in the free jet than the drag predicted in an infinite stream by the exact theory. But this is borne out in his experiments only by the single point, $\sigma = 0$. The linear theory predicts that the drag in a free jet will be lower than in the infinite stream at all cavitation numbers. One feels that this should also appear in the experimental results. If there is an abrupt rise in the drag as the cavitation number increases from zero it certainly should not become greater than the infinite stream value.

*P.W. Brown, "The Force Characteristics of Surface-Piercing, Fully Ventilated, Dihedral Hydrofoils," S.I.T., E.T.T. Rep. No. 698. (To be published).

* * * * *